

Zero temperature DFT and TDDFT for ^4He : A short guide for practitioners

Manuel Barranco,^{1, 2, 3,*} François Coppens,³ Nadine Halberstadt,^{3, †} Alberto Hernando,⁴ Antonio Leal,^{1, 2} David Mateo,⁵ Ricardo Mayol,^{1, 2} and Martí Pi^{1, 2, ‡}

¹*Departament FQA, Facultat de Física,*

Universitat de Barcelona. Diagonal 645, 08028 Barcelona, Spain

²*Institute of Nanoscience and Nanotechnology (IN2UB), Universitat de Barcelona*

³*LCAR-IRSAMC, Université Toulouse 3 and CNRS,*

118 route de Narbonne, F-31062 Toulouse Cedex 09, France

⁴ *Social Thermodynamics Applied Research (SThAR) EPFL
Innovation Park Bâtiment C, CH-1015 Lausanne, Switzerland*

⁵ *Applied Complexity Group, Singapore University of
Technology and Design. 8 Somapah Road, Singapore 487372*

(Dated: July 3, 2017)

Abstract

These are some notes to help the new user understand and use the static and dynamic Barcelona DFT codes for ^4He . With minor changes, the codes can also be employed for the study of other Bose systems, in particular pH₂ clusters and confined cold boson gases. As a preliminary step before opening them to the public, they have been implemented and optimized at CALMIP in Toulouse. Please, refer to them as the 4He-DFT BCN-TLS codes¹. Comments and suggestions are welcome.

Contents

I. Introduction	4
A. Some general considerations	4
B. Available functionals	6
II. Time-independent approach	10
A. General	10
B. Technical details on how the static equations are solved	12
C. Introducing vorticity in the statics	16
III. Dynamics	21
A. Dynamics on a single electronic state	21
B. Impurity-droplet dynamics on multiple electronic states	22
C. Initial conditions	29
D. Technical details on how the dynamic equations are solved	30
E. Absorbing potential at the box boundaries	32
IV. Absorption and emission spectrum within the DF sampling method	34
A. Absorption	35
B. Emission	39
V. The particular case of exciplexes	41
A. A molecular model of the exciplexes	41
B. Exciplex formation within static and time-dependent DFT	43
VI. The test-particle method applied to the solution of the Schrödinger equation for the impurity	43
Acknowledgments	48
A. Convolutions: example of the impurity-He droplet interaction	49
B. Internal units of the programs	51
C. Details on vortex array calculations	53

D. Spectroscopic notation for $L = 1$ excited atomic states in the presence of a ^4He droplet	55
References	56

I. INTRODUCTION

These notes aim at guiding the users of DFT and TDDFT methods to describe complexes made of liquid ${}^4\text{He}$ samples doped with simple impurities. The basic ingredients are the Born-Oppenheimer approximation to factorize the electronic and nuclear wave functions; the Franck-Condon approximation which neglects the dependence of the transition dipole moment with internuclear distance; the short (but not infinitely short) pulse excitation in which the exciting laser pulse is supposed to be short enough that the positions and momenta of the atomic nuclei do not have time to change, but long enough that its energy width only covers one electronic state;^{2–4} and the pairwise additive and diatomics-in-molecule approximation⁵ for describing the interaction energy between the ground and electronically excited dopant and the helium. These ingredients, together with DFT to describe the droplet-impurity complex, allows factorizing the impurity and He nuclear components within the mean field approach. A detailed account of DFT as applied to liquid helium and droplets can be found in Ref.6.

A. Some general considerations

The starting point is to assume that the system is fully Bose-Einstein condensed. For bosons, this is the analogue of considering just one single Slater determinant in the Kohn-Sham approach for fermions. The total energy of the system is written as

$$E[\rho] = \int d\mathbf{r} \{ \mathcal{T}[\rho] + \mathcal{E}_c[\rho] \} \quad (1)$$

where $\rho(\mathbf{r})$ is the helium density, $\mathcal{T}[\rho]$ the kinetic energy density, and $\mathcal{E}_c[\rho]$ is a functional which takes into account the He-He interaction, including exchange and correlation. Several of these functionals are available in the literature.⁶ Writing that all the ${}^4\text{He}$ atoms are in the same single-atom orbital φ_0 , the N -atom wave function is written as

$$\Phi(\mathbf{r}_1, \mathbf{r}_2, \dots, \mathbf{r}_N) = \prod_{i=1}^{i=N} \varphi_0(\mathbf{r}_i) \quad (2)$$

The atom density $\rho(\mathbf{r})$ is the expectation value of the density operator $\hat{\rho} = \sum_{i=1}^{i=N} \delta(\mathbf{r} - \mathbf{r}_i)$:

$$\rho(\mathbf{r}) = \langle \Phi | \hat{\rho} | \Phi \rangle = N |\varphi_0(\mathbf{r})|^2 \quad (3)$$

One usually defines an *order parameter* (some times called *effective wave function*) $\Psi(\mathbf{r})$:

$$\Psi(\mathbf{r}) \equiv \rho^{1/2}(\mathbf{r}) \quad (4)$$

From the previous equations one readily has $\Psi(\mathbf{r}) = \sqrt{N} \varphi_0(\mathbf{r})$. The kinetic energy of the condensate is

$$\mathcal{T}[\rho] = -\frac{\hbar^2}{2m} \sum_i \langle \Phi | \nabla_i^2 | \Phi \rangle = -\frac{\hbar^2}{2m} N \langle \varphi_0 | \nabla^2 | \varphi_0 \rangle \quad (5)$$

where m is the mass of a ${}^4\text{He}$ atom. In terms of $\Psi(\mathbf{r})$ or $\rho(\mathbf{r})$ it can thus be written as

$$\mathcal{T}[\rho] = \frac{\hbar^2}{2m} \int d\mathbf{r} (\nabla \Psi)^2 = \frac{\hbar^2}{2m} \int d\mathbf{r} (\nabla \sqrt{\rho})^2 = \frac{\hbar^2}{2m} \int d\mathbf{r} \frac{1}{4} \frac{(\nabla \rho)^2}{\rho} \quad (6)$$

where we have used integration by parts. If the system has some vorticity the order parameter is complex and related to the particle density as^{7,8}

$$\Psi(\mathbf{r}) \equiv \rho^{1/2}(\mathbf{r}) e^{iS(\mathbf{r})} \quad (7)$$

where the phase $S(\mathbf{r})$ is called the *velocity potential* because it is such that the collective velocity of the superfluid is $\mathbf{v} = (\hbar/m) \nabla S(\mathbf{r})$. As described in section II C page 16, it is possible to handle vortical configurations without much difficulty.^{9–12}

ϵ_{LJ} (K)	σ (\AA)	h (\AA)	c_2 (K \AA^6)	c_3 (K \AA^9)	α_s (\AA^3)
10.22	2.556	2.190323	-2.41186×10^4	1.85850×10^6	54.31
ρ_{0s} (\AA^{-3})	l (\AA)	C (Hartree)	β (\AA^3)	ρ_m (\AA^{-3})	γ_{11}
0.04	1.	0.1	40.	0.37	-19.7544
γ_{12} (\AA^{-2})	α_1 (\AA^{-2})	γ_{21}	γ_{22} (\AA^{-2})	α_2 (\AA^{-2})	
12.5616	1.023	-0.2395	0.0312	0.14912	

TABLE I: Parameters of the OT-DFT and solid functionals.

B. Available functionals

The most accurate and complete functional for ${}^4\text{He}$ is the so-called Orsay-Trento (OT) functional,¹³ whose correlation energy $\mathcal{E}_c[\rho]$ is

$$\begin{aligned} \mathcal{E}_c[\rho] = & \frac{1}{2} \int d\mathbf{r}' \rho(\mathbf{r}) V_{LJ}(|\mathbf{r} - \mathbf{r}'|) \rho(\mathbf{r}') \\ & + \frac{1}{2} c_2 \rho(\mathbf{r}) [\bar{\rho}(\mathbf{r})]^2 + \frac{1}{3} c_3 \rho(\mathbf{r}) [\bar{\rho}(\mathbf{r})]^3 \\ & - \frac{\hbar^2}{4m} \alpha_s \int d\mathbf{r}' F(|\mathbf{r} - \mathbf{r}'|) \left[1 - \frac{\tilde{\rho}(\mathbf{r})}{\rho_{0s}} \right] \nabla \rho(\mathbf{r}) \cdot \nabla' \rho(\mathbf{r}') \left[1 - \frac{\tilde{\rho}(\mathbf{r}')}{\rho_{0s}} \right] \\ & - \frac{m}{4} \int d\mathbf{r}' V_J(|\mathbf{r} - \mathbf{r}'|) \rho(\mathbf{r}) \rho(\mathbf{r}') [\mathbf{v}(\mathbf{r}) - \mathbf{v}(\mathbf{r}')]^2 \end{aligned} \quad (8)$$

In this expression, $\bar{\rho}$ is an averaged density given by

$$\bar{\rho}(\mathbf{r}) = \int d\mathbf{r}' \rho(\mathbf{r}') w(|\mathbf{r} - \mathbf{r}'|) ,$$

where

$$\begin{aligned} w(r) = & \frac{3}{4\pi h^3} \quad \text{if } r < h \\ = & 0 \quad \text{otherwise.} \end{aligned} \quad (9)$$

In addition V_{LJ} is a finite range interaction consisting of a Lennard-Jones (LJ) potential with truncated core

$$\begin{aligned} V_{LJ}(r) = & 4\epsilon_{LJ} \left[\left(\frac{\sigma}{r} \right)^{12} - \left(\frac{\sigma}{r} \right)^6 \right] \quad \text{if } r > h \\ = & 0 \quad \text{otherwise.} \end{aligned} \quad (10)$$

A Gaussian kernel

$$F(r) = \frac{1}{\pi^{3/2} l^3} e^{-r^2/l^2}$$

is used to define the other averaged density entering \mathcal{E}_c :

$$\tilde{\rho}(\mathbf{r}) = \int d\mathbf{r}' \rho(\mathbf{r}') F(|\mathbf{r} - \mathbf{r}'|) .$$

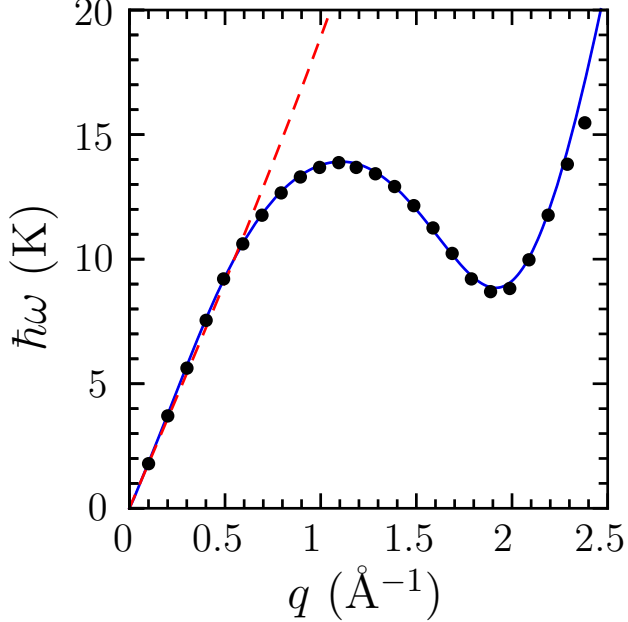


FIG. 1: Dispersion relation of the elementary excitations in bulk liquid ^4He at $T = 0$. Solid line: OT results. Dashed line: results using the functional of Refs. 18,19. Dots: Experimental data from Ref. 14 (*by courtesy of F. Ancilotto, University of Padova*).

The last term of Eq. (8) mimics the back flow contribution, where $V_J(r)$ is an effective current-current interaction fitted so as to reproduce the maxon-roton dispersion curve in liquid ^4He ¹³

$$V_J(r) = (\gamma_{11} + \gamma_{12} r^2)e^{-\alpha_1 r^2} + (\gamma_{21} + \gamma_{22} r^2)e^{-\alpha_2 r^2} \quad (11)$$

and the velocity is defined as $\mathbf{v}(\mathbf{r}) = \mathbf{j}(\mathbf{r})/\rho(\mathbf{r})$, where the current is

$$\mathbf{j}(\mathbf{r}) = -\frac{i\hbar}{2m}[\Psi^*(\mathbf{r})\nabla\Psi(\mathbf{r}) - \Psi(\mathbf{r})\nabla\Psi^*(\mathbf{r})] \quad (12)$$

The OT functional gives a quite accurate description of inhomogeneous configurations of liquid ^4He at $T = 0$, as can be seen from Fig. 1. However, its full version is seldom used in applications to inhomogeneous systems.¹⁵ In most dynamic applications, the back flow term is neglected because of its complexity. This term has no effect on the statics and has been found to be unstable in some dynamic applications for still unknown reasons. The α_s non-local kinetic energy correction term is sometimes not included although it is stable and can be handled in the dynamics. The effect of the non-local kinetic energy and back flow terms on the elementary excitation spectrum of liquid helium at zero temperature (T) can be found in Ref. 16. It is illustrated in Fig. 2, which compares the results of a DFT

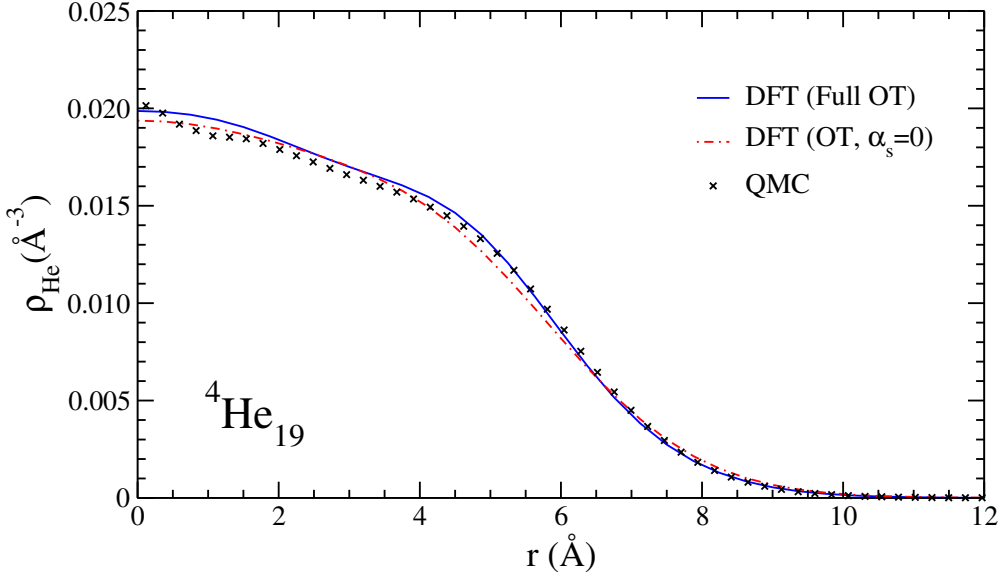


FIG. 2: Comparison between OT DFT (total or with $\alpha_s = 0$) and QMC calculations for the density profile of a ${}^4\text{He}_{19}$ droplet. See Eq. (8) and the discussion in the paragraph following Eq. (12) for the meaning and the importance of the non-local kinetic energy correction term in α_s . The QMC calculation has been carried out by M. Rossi, University of Padova.

simulation using the full OT version and the ones obtained by setting $\alpha_s = 0$ with the ones from a QMC simulation in the case of a ${}^4\text{He}_{19}$ droplet. As can be seen from that figure, even in the case of such a small droplet, DFT gives a quite accurate description, and the effect of neglecting the non-local kinetic energy term is small.

The OT functional is unstable when very attractive impurities are doping the liquid, because of the appearance of very structured liquid densities around them. A simplified version has been proposed to overcome this limitation at the price of not including the back flow nor the non-local kinetic energy terms.¹⁷ Originally, this functional was devised to address the freezing of ${}^4\text{He}$ and its liquid-solid interface and for this reason we will refer to it as the “solid” functional. Its structure is the following:

$$\begin{aligned} \mathcal{E}_c[\rho] &= \frac{1}{2} \int d\mathbf{r}' \rho(\mathbf{r}) V_{LJ}(|\mathbf{r} - \mathbf{r}'|) \rho(\mathbf{r}') + C \rho(\mathbf{r}) \{1 + \tanh(\beta[\rho(\mathbf{r}) - \rho_m])\} \\ &+ \frac{1}{2} c_2 \rho(\mathbf{r}) \bar{\rho}^2(\mathbf{r}) + \frac{1}{3} c_3 \rho(\mathbf{r}) \bar{\rho}^3(\mathbf{r}) \end{aligned} \quad (13)$$

The second term in Eq. (13) is a “penalty term” to avoid unphysical piling-up of helium atoms that appear *e.g.* around very attractive impurities such as cations in the form of solid-like structures, characterized by a highly inhomogeneous, very structured density dis-

tribution with unphysically large density values. This term only acts when the density is large, of the order of a predefined value ρ_m , contributing to the effective potential felt by the liquid with a term which acts as a repulsive barrier that forbids extra pile-up of the density. By construction, such term has no effect whatsoever on the liquid structure. The parameters defining the OT and solid functionals are collected in Table I. The computing package has both functionals as possible options.

In some particular applications the finite-range of the He-He interaction is of minor relevance and one may resort to a much simpler zero-range interaction that was at the origin of the density functional approach to liquid He.^{18,19} This functional is not in the package although it can be easily included. Due to its simplicity it has been used to address the statics and dynamics of electron bubbles in liquid helium.²⁰

Let us mention that a simplified version of the OT functional has been extended to finite temperatures below the lambda point,²¹ and that a zero temperature, finite range functional for ³He-⁴He mixtures is also available.²² It was used to address mixed droplets doped with OCS.²³ Different functionals for pristine ³He are also available and have been used in the past, see *e.g.* Refs. 24,25 and references therein. Finally, the package can be easily adapted to describe cold dipolar Bose gases²⁶ (and in general, anything admitting a static or dynamic Gross-Pitaevskii mean field description) and parahydrogen clusters, for which a DFT approach is also available.²⁷

II. TIME-INDEPENDENT APPROACH

A. General

The ground state structure of the system is obtained solving the Euler-Lagrange (EL) equation resulting from the functional variation of the total energy $E[\rho]$ with respect to either ρ or Ψ under the condition of a fixed number of ${}^4\text{He}$ atoms. Variation with respect to Ψ gives an EL equation that looks very similar to a Schrödinger equation for the order parameter

$$\left\{ -\frac{\hbar^2}{2m} \nabla^2 + \frac{\delta \mathcal{E}_c}{\delta \rho} \right\} \Psi(\mathbf{r}) \equiv \mathcal{H}[\rho] \Psi(\mathbf{r}) = \mu \Psi(\mathbf{r}) \quad (14)$$

where μ is the chemical potential that is unknown for a droplet. For bulk liquid helium μ is known in advance from the equation of state of the liquid that is embodied in \mathcal{E}_c .⁹ This is so even in the presence of impurities, or for the free-surface of the liquid, since away from the surface or the impurity the system tends to the bulk liquid and the chemical potential is the same all over space.

A “point-like” impurities interacting with He is introduced as an external field acting on the superfluid if the impurity is “much more” massive than He; otherwise it is treated as a quantum object described by a Schrödinger equation. In both cases, one has to know the impurity-He atom interaction $V_{\text{He}-I}$; the impurity-droplet interaction is handled in the pairwise sum approximation. The changes that have to be introduced in the formalism are obvious. In the case of a classical impurity, one simply adds to $E[\rho]$ the impurity-droplet interaction energy

$$E[\rho] \rightarrow E[\rho] + \int d\mathbf{r} \rho(\mathbf{r}) V_{\text{He}-I}(|\mathbf{r} - \mathbf{r}_I|) \quad (15)$$

where \mathbf{r}_I is the position of the impurity. The helium distribution is then obtained by solving the EL equation

$$\left\{ -\frac{\hbar^2}{2m} \nabla^2 + \frac{\delta \mathcal{E}_c}{\delta \rho} + V_{\text{He}-I}(|\mathbf{r} - \mathbf{r}_I|) \right\} \Psi(\mathbf{r}) = \mu \Psi(\mathbf{r}) \quad (16)$$

In the case of a quantum impurity, $E[\rho]$ has to be modified in order to take into account the zero point motion of the impurity

$$E[\rho] \rightarrow E[\rho] + \frac{\hbar^2}{2m_I} \int d\mathbf{r}_I |\nabla_{\mathbf{r}_I} \phi(\mathbf{r}_I)|^2 + \iint d\mathbf{r} d\mathbf{r}_I \rho(\mathbf{r}) V_{\text{He}-I}(|\mathbf{r} - \mathbf{r}_I|) |\phi(\mathbf{r}_I)|^2 \quad (17)$$

where $\phi(\mathbf{r}_I)$ is the wave function of the impurity and m_I its mass. In this case, one has to solve two coupled Schrödinger-like equations

$$\left\{ -\frac{\hbar^2}{2m} \nabla_{\mathbf{r}}^2 + \frac{\delta \mathcal{E}_c}{\delta \rho} + \int d\mathbf{r}_I V_{\text{He}-I}(|\mathbf{r} - \mathbf{r}_I|) |\phi(\mathbf{r}_I)|^2 \right\} \Psi(\mathbf{r}) = \mu \Psi(\mathbf{r}) \quad (18a)$$

$$\left\{ -\frac{\hbar^2}{2m_I} \nabla_{\mathbf{r}_I}^2 + \int d\mathbf{r} V_{\text{He}-I}(|\mathbf{r} - \mathbf{r}_I|) \rho(\mathbf{r}) \right\} \phi(\mathbf{r}_I) = \varepsilon \phi(\mathbf{r}_I), \quad (18b)$$

The DFT programs can also provide the minimum energy configuration as a function of the distance \mathcal{Z}_0 between the center of mass (COM) of the helium droplet and the impurity (with the z axis chosen along the He COM - impurity direction). This is done by adding a constraint to any of the previous energy expressions, minimizing *e.g.* the expression

$$E[\rho] + \int d\mathbf{r} \rho(\mathbf{r}) V_{\text{He}-I}(|\mathbf{r} - \mathbf{r}_I|) + \frac{\lambda_C}{2} [\mathcal{Z} - \mathcal{Z}_0]^2 \quad (19)$$

where \mathcal{Z} is the distance between the impurity and the center of mass of the helium droplet and \mathcal{Z}_0 its target value, and λ_C is an arbitrary constant. Values of λ_C in the $1000 - 3000$ K Å⁻² range have been used to ensure that the desired \mathcal{Z}_0 value is obtained within a 0.1% accuracy.

Let us illustrate how the EL equations, Eqs. (18), are changed for a quantum impurity, when adding a constraint on its position. Defining the helium COM and impurity positions,

$$\begin{aligned} Z_{CM} &= \frac{1}{N} \int d\mathbf{r} z \rho(\mathbf{r}) \\ z_{imp} &= \int d\mathbf{r}_I z_I |\phi(\mathbf{r}_I)|^2, \end{aligned} \quad (20)$$

$\mathcal{Z} = z_{imp} - Z_{CM}$ and Eqs. (18) become

$$\begin{aligned} \left\{ -\frac{\hbar^2}{2m} \nabla_{\mathbf{r}}^2 + \frac{\delta \mathcal{E}_c}{\delta \rho} + \int d\mathbf{r}_I V_{\text{He}-I}(|\mathbf{r} - \mathbf{r}_I|) |\phi(\mathbf{r}_I)|^2 + \lambda_C [\mathcal{Z} - \mathcal{Z}_0] \left(\frac{-z}{N} \right) \right\} \Psi(\mathbf{r}) &= \mu \Psi(\mathbf{r}) \\ \left\{ -\frac{\hbar^2}{2m_I} \nabla_{\mathbf{r}_I}^2 + \int d\mathbf{r} V_{\text{He}-I}(|\mathbf{r} - \mathbf{r}_I|) \rho(\mathbf{r}) + \lambda_C [\mathcal{Z} - \mathcal{Z}_0] z_I \right\} \phi(\mathbf{r}_I) &= \varepsilon \phi(\mathbf{r}_I) \end{aligned} \quad (21)$$

In the case of a classical impurity one simply adds $\lambda_C [\mathcal{Z} - \mathcal{Z}_0] (-z_I/N)$ to the left hand side of Eq. (16), z_I being the impurity position.

B. Technical details on how the static equations are solved

The static DFT equations are always solved in cartesian coordinates. The calculation is full 3D with no imposed symmetry whatsoever. Densities, wave functions and differential operators are discretized on a 3D cartesian grid (“*calculating box*”). The minimum and maximum values of x , y , and z for the calculating box are inputs to the programs, as well as the number of points in each direction n_i . The limits of the calculating box have to be chosen with care, especially if a dynamic calculation follows the (relatively fast) static minimization. One has to make sure that in the course of the dynamics there will be enough room for the droplet and the impurity to wander around without hitting the cell boundaries before obtaining the desired information. The number of points in each direction has to be chosen such that the FFT is efficiently calculated (see below) and that the size step is about the desired value. We typically use a size step $h_x = (x_{max} - x_{min})/n_x$, etc..., of the order of 0.4 Å.

The differential operators (usually first and second derivatives at most) are represented by k -point formulas. We normally use 13-point formulas, but values up to $k = 25$ are also possible. We have found that increasing the number of points for the derivatives does not improve the numerics –but it increases the CPU time! Decreasing the spatial step can result in a non affordable calculation (too much computing time and too large memory required).

A key tool for the implementation of the method is the use of fast-Fourier techniques²⁸ to calculate the convolutions needed to obtain some of the contributions to the total energy of the impurity-droplet complex, as well as the mean field potentials entering the EL equations for the order parameter and the impurity wave function. In order to accelerate the computations, the Fourier transforms of the He-He and He-impurity potentials and of the expressions entering the definition of the coarse-grained helium density in the functional^{13,17} are computed once and for all at the beginning of the calculation. The method is detailed in Appendix A.

Eqs. (16) or (18) is solved by the imaginary time method (ITM),^{29,30} that schematically goes as follows. Let us consider the following time-dependent Schrödinger equation

$$i\hbar \frac{\partial}{\partial t} \psi = \mathcal{H}\psi \quad (22)$$

It can be formally integrated for a time interval δt yielding

$$\psi(\delta t) = e^{-i\frac{\delta t}{\hbar}\mathcal{H}}\psi(0) \quad (23)$$

Let us expand $\psi(0)$ in eigenfunctions ϕ_k of the Hamiltonian \mathcal{H} , with energy ϵ_k

$$\psi(0) = \sum_{k=0}^{k=\infty} c_k \phi_k \quad (24)$$

Hence,

$$\psi(\delta t) = \sum_{k=0}^{k=\infty} c_k e^{-i\frac{\delta t}{\hbar}\epsilon_k} \phi_k \quad (25)$$

Any time interval is obtained by setting $t = n\delta t$ and making n as large as needed,

$$\psi(t) = \psi(n\delta t) = \sum_{k=0}^{k=\infty} c_k e^{-i\frac{n\delta t}{\hbar}\epsilon_k} \phi_k \quad (26)$$

By setting $\delta t \equiv -i\hbar\delta\tau$ (τ is called “*imaginary time*”), it is obtained

$$\psi(\tau) = \psi(n\delta\tau) = \sum_{k=0}^{k=\infty} c_k e^{-n\delta\tau\epsilon_k} \phi_k = \sum_{k=0}^{k=\infty} c_k e^{-\tau\epsilon_k} \phi_k \quad (27)$$

For long enough τ 's, only the component ϕ_0 corresponding to the lowest eigenvalue ϵ_0 “survives”. The ITM thus yields the ground state of the system provided that the initial guess $\psi(0)$ used to start the minimization is “reasonable enough”, *i.e.* it is not orthogonal to the ground state.

The initial guess for the helium density depends on the nature of the system (droplet or bulk liquid) and, in the case of a droplet, on the expected equilibrium position of the impurity.

(i) *For a pure helium droplet, the initial density $\rho_o(r)$ is taken as proportional to $1/(1 + \exp[(r - R)/a])$ where r is measured from the center of the droplet, R is the droplet radius estimated from a sphere with homogeneous, constant density equal to that of the bulk, and a is a measure of the surface thickness, taken to be of the order of 0.5 Å.*

(ii) *If the He-impurity interaction is very attractive, the impurity is expected to be solvated and hence it is initially positioned at the center of the droplet. The initial guess for the helium density is then taken as that of a pure helium droplet*

of the same size in which a spherical hole has been drilled at its center. The radius of the hole is taken as the distance at which the He-impurity potential is zero (repulsive wall). The rest of the helium density is then multiplied by the appropriate factor in order to normalize it to the desired number of atoms.

(iii) For a solvated impurity in bulk helium, a hole is drilled at the center of the simulation box in the bulk helium density, which is left constant at its equilibrium bulk value everywhere else.

(iv) If the He-impurity interaction is less attractive, so that it is expected to sit in a dimple near the surface (see also Ancilotto's parameter³¹), the impurity is initially located at or near the surface and a hole is drilled in the helium density from (i).

(v) If in addition the impurity is treated quantum mechanically, the initial guess for its wave function is taken as a gaussian positioned at the position the impurity would have if treated classically. Its width parameter is set to about 1 Å.

Note that the explicit values of these initial parameters are not critical since they will be optimized with the ITM. It is only required that the initial density be normalized to the number of He atoms in the cases of a droplet.

In order to solve for the ITM equations in practice, Eq. (23) is approximated to the first order in $\delta\tau$ (although one could go to higher order, this is not the way it is implemented) writing

$$\psi(\tau + \delta\tau) \simeq (1 - \delta\tau\mathcal{H})\psi(\tau) \equiv \psi(\tau) + \delta\psi(\tau) \quad (28)$$

This expression is iterated until convergence. Notice that unitarity is lost in Eq. (27) because time is imaginary. Hence ψ has to be normalized after each iteration.

This method yields the eigenvector but not the eigenvalue. The chemical potential of the droplet is obtained from the expectation value of the Hamiltonian, $\mu = \langle\Psi|\mathcal{H}|\Psi\rangle/\langle\Psi|\Psi\rangle \equiv \langle\mathcal{H}\rangle/\langle\Psi|\Psi\rangle$. The calculation of the impurity wave function proceeds in a similar way.

In practice, the convergence of the procedure is checked on the total energy of the complex, Eq. (15) for instance. Other tests are done in the course of the minimization, as for instance a comparison between the point-by-point, local chemical potential $\mu(\mathbf{r}) = (\mathcal{H}|\Psi\rangle)/\Psi(\mathbf{r})$ and its integrated value above. It is worth pointing out that the ITM is very simple to implement, since it just involves the repeated application of the Hamiltonian operator on the order parameter.

Since the Hamiltonian itself depends on the order parameter, the time step $\delta\tau$ cannot be made too large. Eq. (28) shows that the ITM belongs to the general class of relaxation

methods employed to solve partial differential equations (a parabolic partial differential equation).³² This provides a hint for fixing $\delta\tau$ in such a way that the imaginary time evolution is stable, namely $\hbar^2\delta\tau_{max}/(2m\Delta^2) < 1/2$, with Δ the smallest between the x, y and z space steps.³² In actual calculations we have taken $\delta\tau = 0.1\delta\tau_{max}$ at most; a typical factor is 0.05 instead of 0.1; in the presence of fairly attractive impurities, $\delta\tau$ is often reduced to $10^{-3}\delta\tau_{max}$, at least for the first iterations. The possibility of using a small time-step for the first iterations and increase it next is implemented (this is actually a trial-and-error procedure). Note that using a smaller space step does not result in the possibility of using *larger* time steps; from the stability criterium, it is rather the opposite!

From the previous discussion and since upon convergence $(\mathcal{H} - \mu)\Psi = 0$, the following expression for $\Delta\psi(\tau)$

$$\delta\Psi(\tau) = -\frac{\delta\tau(\mathcal{H} - \mu)}{1 - \delta\tau(\langle\mathcal{H}\rangle - \mu)} \Psi(\tau) \quad (29)$$

has the advantage of making the change in Ψ smaller as one approaches convergence. In Eq. (29), μ is taken as the value of $\langle\psi|H|\psi\rangle$ at the preceding iteration. The above iteration scheme implies that at this stage, $\psi(\tau)$ is normalized to unity up to order $\delta\tau$. Once evolved to $\psi(\tau + \delta\tau)$, it has to be normalized to N .

In the case of the bulk liquid or free liquid surface, the chemical potential μ is known in advance and the relaxation procedure goes as

$$\psi(\tau + \delta\tau) \simeq \frac{1 - \delta\tau\mathcal{H}}{1 - \delta\tau\mu} \psi(\tau) \quad (30)$$

In this case, normalization means that $\rho(\mathbf{r}) \rightarrow \rho_b$ at the boundaries of the calculation cell, where ρ_b is the bulk equilibrium density. The starting He configuration also needs to have this information built in: this is similar to starting the iteration for a droplet with a density profile normalized to the desired number of atoms. Notice that for this to be possible, the calculation cell has to be large enough.

To speed up the solution of the EL equations, we use the preconditioning smoothing operation described in Ref. 33, that is adapted as follows (the x, y and z coordinates are

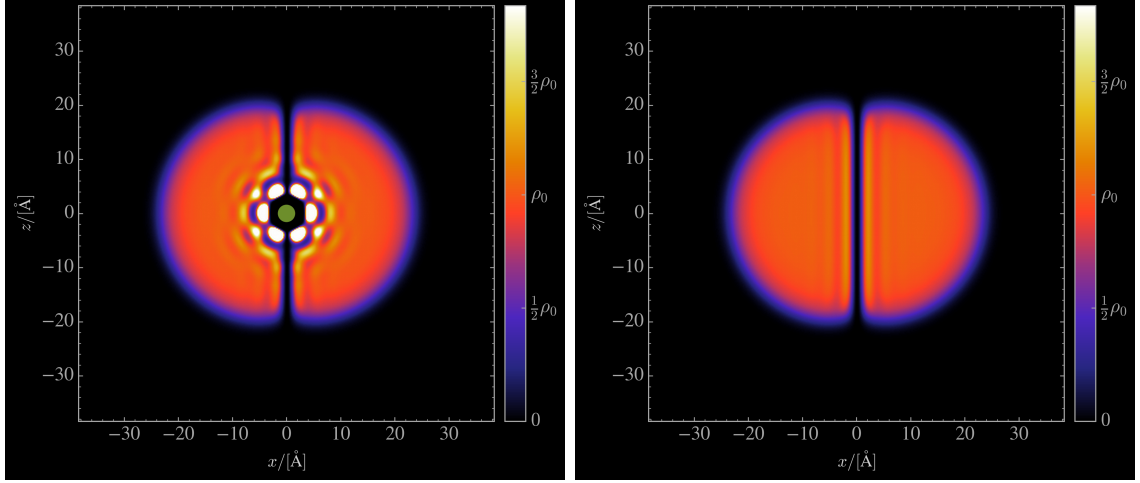


FIG. 3: Helium density in the $x = 0$ plane corresponding to the $\text{Xe}@\text{He}_{1000}$ (left) and pure He_{1000} (right) droplets hosting a vortex line.

now explicated):

$$\begin{aligned} \delta\Psi(x, y, z, \tau) \rightarrow \overline{\delta\Psi(x, y, z, \tau)} &\equiv \frac{1}{2}\delta\Psi(x, y, z, \tau) \\ &+ \frac{1}{12}\{\delta\Psi(x \pm \delta x, y, z, \tau) + \delta\Psi(x, y \pm \delta y, z, \tau) + \delta\Psi(x, y, z \pm \delta z, \tau)\} \end{aligned} \quad (31)$$

The performance of the code has been further improved by adding a “viscosity term” to the correction $\delta\Psi(\tau)$ to the order parameter, *i.e.*,

$$\delta\Psi(\tau) \rightarrow \overline{\delta\Psi(\tau)} + \alpha_{V_1}[\Psi(\tau) - \Psi(\tau - \delta\tau)] + \alpha_{V_2}[\Psi(\tau - \delta\tau) - \Psi(\tau - 2\delta\tau)] \quad (32)$$

The heuristic viscosity parameters α_{V_1} and α_{V_2} are fixed to a value of 0.6 and 0.1, respectively. These last two tricks allow one to use larger time-steps, and therefore to speed up convergence.

C. Introducing vorticity in the statics

As mentioned before, if the droplet hosts some vorticity the effective helium wave function must be complex; otherwise, no currents may appear in the superfluid. For a helium droplet axially symmetric around the z axis, the following order parameter

$$\Psi(r, \theta) \equiv \rho^{1/2}(r) e^{im\theta} \quad (33)$$

defines a vortex line along the z -axis, where r is the distance to the symmetry axis, θ the polar angle and m is the circulation number. One may see that it is an eigenvector of the total angular momentum operator $\hat{L}_z = -i\hbar\partial/\partial\theta$ and that the angular momentum in the droplet is

$$\langle \hat{L}_z \rangle = \langle \Psi(r, \theta) | \hat{L}_z | \Psi(r, \theta) \rangle = Nm\hbar \quad (34)$$

In practice, only configurations with circulation $m = 1$ are relevant, since the ones with higher m values are energetically unstable and decay.

The EL equations to be solved are the same ones as in the case of vortex-free droplets [Eqs. (14) and (16)], but the effective wave function is now complex. It turns out that in order to produce a linear vortex along the symmetry axis of the system (pure droplet or doped droplet with the impurity along the symmetry axis), one just has to start the imaginary time iteration from a helium density in which the vortex line has been “imprinted”. For instance, a vortex line along the z axis can be produced by starting the imaginary time relaxation from the effective wave function

$$\Psi(\mathbf{r}) = \frac{\rho_0^{1/2}(\mathbf{r})}{\sqrt{x^2 + y^2}} (x + iy) \quad (35)$$

where $\rho_0(\mathbf{r})$ is the density corresponding to either the pure or to the doped droplet without vortex. More involved imprinted configurations can be found in *e.g.* Refs. 9,11. As an example, Fig. 3 shows a vortex line in ${}^4\text{He}_{1000}$ and $\text{Xe} @ {}^4\text{He}_{1000}$ droplets. Pure and doped droplets hosting vortices can be characterized by different energies;^{9,11,12} let us mention the following ones:

- *Solvation energy* of the impurity X :

$$S_X = E(X @ {}^4\text{He}_N) - E({}^4\text{He}_N)$$

- *Vortex (V) energy*:

$$E_V = E(V @ {}^4\text{He}_N) - E({}^4\text{He}_N)$$

- *Binding energy* of the impurity *to the vortex*, also called “*substitution energy*”:⁷

$$B_X = \{E(X @ {}^4\text{He}_N) - E({}^4\text{He}_N)\} - \{E[(X + V) @ {}^4\text{He}_N] - E(V @ {}^4\text{He}_N)\}$$

In general, atomic impurities are barely attached to the vortex line. For instance, it has been found that Xe is bound to the vortex line by about 3-5 K.^{10,12} It is worth seeing that B_X arises from the subtraction of fairly large numbers, which makes its accurate evaluation rather complex. If instead of a vortex line one has to generate vortex arrays, the strategy is different: one works in the fixed-droplet frame of reference (corotating frame) and looks for solutions of the following EL equation:

$$[\hat{H} - \omega \hat{L}_z] \Psi(\mathbf{r}) = \mu \Psi(\mathbf{r}) , \quad (36)$$

where \hat{H} is the DFT Hamiltonian,¹⁷ \hat{L}_z is the angular momentum operator around the z -axis, and ω is the angular velocity of the corotating frame. In this case, $\Psi(\mathbf{r})$ no longer is an eigenvector of the angular momentum.

In order to determine $\Psi(\mathbf{r})$ for a configuration where N_v vortex lines are present one can follow again the imprinting strategy. The imaginary-time evolution of Eq. (36) leading to the minimum energy configuration is then initialized with the helium wave function

$$\Psi(\mathbf{r}) = \rho_0^{1/2}(\mathbf{r}) \prod_{j=1}^{N_v} \left[\frac{(x - x_j) + i(y - y_j)}{\sqrt{(x - x_j)^2 + (y - y_j)^2}} \right] \quad (37)$$

where $\rho_0(\mathbf{r})$ is the density of the vortex-free droplet and (x_j, y_j) is the initial position of the j -vortex linear core with respect to the z -axis of the droplet (note that $\Psi(\mathbf{r})$ was incorrectly written in Refs. 10,11). During the functional minimization the vortex positions will change to provide, at convergence, the lowest energy vortex configuration for the given angular velocity ω .

Note that the angular velocity does not get into the EL equation for one single vortex. The critical angular velocity for nucleating a vortex line in a droplet made of N helium atoms is

$$\omega_c = \frac{1}{\hbar} \frac{E_V}{N} \quad (38)$$

where E_V is the vortex energy as defined above.³⁴ Using the values for the ${}^4\text{He}_{1000}$ droplet we have

$$\omega_{c({}^4\text{He}_{1000})} = \frac{0.1272 \text{ K}}{7.638235 \text{ K ps}} = 0.0167 \text{ ps}^{-1} . \quad (39)$$

Some details on units are presented in Appendix C page 53.

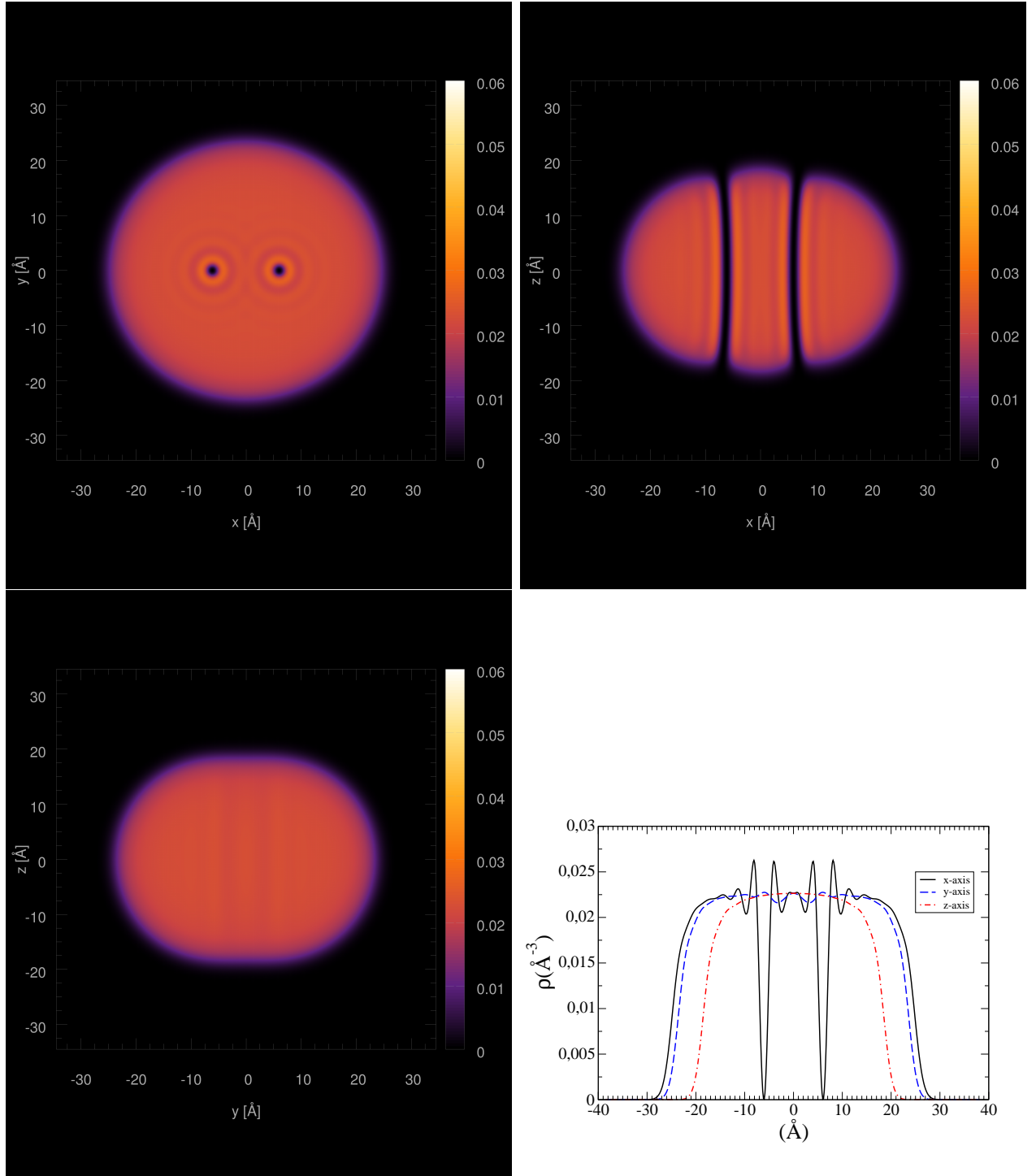


FIG. 4: Two-vortex configuration “parallel” to the z -axis for the ${}^4\text{He}_{1000}$ droplet at angular velocity $\omega = 0.175 \text{ K}/\hbar = 0.0229 \text{ ps}^{-1}$. Top left: density in the (x, y) plane; top right: density in the (x, z) plane. Bottom left: density in the (y, z) plane; bottom right: density profiles along the x , y and z axes .

Fig. 4 shows the two-vortex configuration at angular frequency $\omega = 0.175 \text{ K}/\hbar = 0.0229 \text{ ps}^{-1}$. The angular momentum is $\langle \hat{L}_z \rangle \sim 1836$. Notice the bending of the vortex line so as to hit the droplet surface perpendicularly, and the flattening out of the droplet in the z direction because of the “centrifugal force”.

III. DYNAMICS

In this section we describe how to simulate a dynamics process involving a dopant and a helium droplet or bulk liquid helium. In all applications of the method made so far, the dynamics has been triggered either by photoionization or photoexcitation of the impurity, or by dopant-helium droplet collision.

Once the static configuration has been obtained, several choices have to be made for the dynamics. Like for the static study, a light impurity requires a quantal description, while classical dynamics is sufficient for a heavy one. Also, depending on the process, dynamics evolves on a single potential energy surface or it can involve several coupled electronic states.

A. Dynamics on a single electronic state

This section is dedicated to the simulation of dynamical processes involving a single electronic state of the dopant. The simplest case is that in which the impurity can be treated classically. This is the case, for instance, of the dynamics triggered by excitation of a heavy alkali atom (Rb, Cs) from the ns ground state to the $(n+1)s$ excited state,³⁵ or of the dynamics triggered by the photoionization of a Ba atom³⁶ (see also Ref. 37), or of collision dynamics between a helium droplet and an impurity to study pickup and solvation of dopants.³⁸ Both the photoexcitation or photoionization processes are considered as instantaneous.⁶²

After ionization or excitation, or at the beginning of the collision, the total energy of the complex is written as

$$E[\Psi, \mathbf{r}_I(t)] = \int d\mathbf{r} \frac{\hbar^2}{2m} |\nabla \Psi|^2 + \frac{p_I^2(t)}{2m_I} + \int d\mathbf{r} \mathcal{E}_c(\rho) + \int d\mathbf{r} \rho(\mathbf{r}, t) V_{\text{He}-I}(|\mathbf{r} - \mathbf{r}_I(t)|), \quad (40)$$

where I stands for the impurity, p_I its classical momentum, and $V_{\text{He}-I}$ is the interaction pair potential between a helium atom and the impurity in its appropriate electronic state: excited (photoexcitation) or ionized (photoionization), or in the ground, excited or ionized state depending on the nature of the collision studied. The order parameter is now a complex function $\Psi(\mathbf{r}, t)$ and the position of I , $\mathbf{r}_I(t)$, is treated classically. Thus, $\Psi(\mathbf{r}, t)$ is evolved

following the TDDFT prescription and $\mathbf{r}_I(t)$ according to Newton's law:

$$i\hbar \frac{\partial}{\partial t} \Psi = \left[-\frac{\hbar^2}{2m} \nabla_{\mathbf{r}}^2 + \frac{\delta \mathcal{E}_c}{\delta \rho} + V_{\text{He}-I}(|\mathbf{r} - \mathbf{r}_I|) \right] \Psi \quad (41a)$$

$$m_I \ddot{\mathbf{r}}_I = -\nabla_{\mathbf{r}_I} \left[\int d\mathbf{r} \rho(\mathbf{r}, t) V_{\text{He}-I}(|\mathbf{r} - \mathbf{r}_I|) \right] = - \int d\mathbf{r} V_{\text{He}-I}(|\mathbf{r} - \mathbf{r}_I|) \nabla_{\mathbf{r}} [\rho(\mathbf{r}, t)] . \quad (41b)$$

where the time dependence of the parameters is omitted for the sake of clarity, except when needed. For a light impurity under the same conditions, Eqs. (40) and (41) have to be changed to

$$\begin{aligned} E[\Psi, \Phi] = & \int d\mathbf{r} \frac{\hbar^2}{2m} |\nabla_{\mathbf{r}} \Psi|^2 + \int d\mathbf{r}_I \frac{\hbar^2}{2m_I} |\nabla_{\mathbf{r}_I} \Phi|^2 + \int d\mathbf{r} \mathcal{E}_c(\rho) \\ & + \iint d\mathbf{r} d\mathbf{r}_I \rho(\mathbf{r}, t) V_{\text{He}-I}(|\mathbf{r} - \mathbf{r}_I|) |\phi(\mathbf{r}_I, t)|^2 \end{aligned} \quad (42)$$

and

$$i\hbar \frac{\partial}{\partial t} \Psi(\mathbf{r}, t) = \left[-\frac{\hbar^2}{2m} \nabla_{\mathbf{r}}^2 + \frac{\delta \mathcal{E}_c}{\delta \rho} + \int d\mathbf{r}_I V_{\text{He}-I}(|\mathbf{r} - \mathbf{r}_I|) |\phi(\mathbf{r}_I, t)|^2 \right] \Psi(\mathbf{r}, t) \quad (43a)$$

$$i\hbar \frac{\partial}{\partial t} \phi(\mathbf{r}_I, t) = \left[-\frac{\hbar^2}{2m_I} \nabla_{\mathbf{r}_I}^2 + \int d\mathbf{r} V_{\text{He}-I}(|\mathbf{r} - \mathbf{r}_I|) \rho(\mathbf{r}, t) \right] \phi(\mathbf{r}_I, t) , \quad (43b)$$

respectively, where $\phi(\mathbf{r}_I, t)$ is the wave function of the impurity. In cases where the impurity is ejected with a high kinetic energy, the time scales for the evolution of the light impurity and for the helium droplet are fairly different. In order to have a stable evolution, one should then use the smaller time step, which is the one corresponding to the light impurity. In addition, the description of the impurity also requires a fine mesh in this case. These two aspects can make the calculation unaffordable. One way out of this problem has been to simulate the solution of the Schrödinger equation of the impurity using test particles.³⁹ This has been done in Ref. 40 for droplets doped with Na and Li atoms whose dynamics has been triggered by $ns \rightarrow (n+1)s$ excitation of the dopant. The code is available, but is not in the computing package yet.

B. Impurity-droplet dynamics on multiple electronic states

A more complex situation arises when several coupled electronic states of the impurity

are involved in the dynamics. This is the case when a simple impurity is dipolarly excited from an ns to an $n'p$ state, for instance. The three degenerate $L = 1$ states of the atom are split by the interaction with a helium atom into a Σ ($\Lambda = 0$) and a doubly degenerate Π ($\Lambda = \pm 1$) state, Λ being the projection quantum number of the atomic orbital angular momentum \mathbf{L} on the interatomic axis. In this case, the electronic state of the impurity must be explicitly incorporated into the dynamics because it can evolve during the simulation. Let us consider the case where the impurity can be treated as a classical particle because of its large mass.⁴¹ First, one has to build the He-impurity interaction in order to describe the droplet-impurity interaction. The method is based on the diatomics in molecules (DIM) model⁵ and it is presented in detail in Ref. 42. It basically goes as follows.

The electronic structure of the $n'p$ excited impurity is approximated by a one-electron excitation in the basis of effective p orbitals. Using the $|p_{x'n}\rangle$, $|p_{y'n}\rangle$, $|p_{z'n}\rangle$ orbitals in the cartesian (x'_n, y'_n, z'_n) frame with its z'_n axis parallel to the distance vector \mathbf{r}'_n between the impurity and the n^{th} helium atom, its interaction with this (s-state) helium atom can be expressed as

$$\begin{aligned} U(r'_n) &= \begin{pmatrix} V_\Pi(r'_n) & 0 & 0 \\ 0 & V_\Pi(r'_n) & 0 \\ 0 & 0 & V_\Sigma(r'_n) \end{pmatrix} \\ &= V_\Pi(r'_n)\{|p_{x'n}\rangle\langle p_{x'n}| + |p_{y'n}\rangle\langle p_{y'n}|\} + V_\Sigma(r'_n)|p_{z'n}\rangle\langle p_{z'n}| \\ &= V_\Pi(r'_n)\mathbf{I} + \{V_\Sigma(r'_n) - V_\Pi(r'_n)\}|p_{z'n}\rangle\langle p_{z'n}|, \end{aligned} \quad (44)$$

where $V_\Pi(r')$ and $V_\Sigma(r')$ are the $\Lambda = \pm 1$ and $\Lambda = 0$ He-impurity adiabatic pair potentials neglecting the spin-orbit interaction. For alkali-like atoms the V_Σ potential is repulsive except for a possible shallow Van der Waals well at long distances, while the V_Π potential usually has a rather deep well at short distances. Fig. 5 shows the He-K pair potentials as an illustration.

If referenced to another system of axes in which the z axis is not necessarily parallel to the He-I axis denoted as z'_n , the U matrix is given by

$$U = V_\Pi(r'_n)\mathbf{I} + [V_\Sigma(r'_n) - V_\Pi(r'_n)]R_n|p_{z'_n}\rangle\langle p_{z'_n}|R_n^{-1}, \quad (45)$$

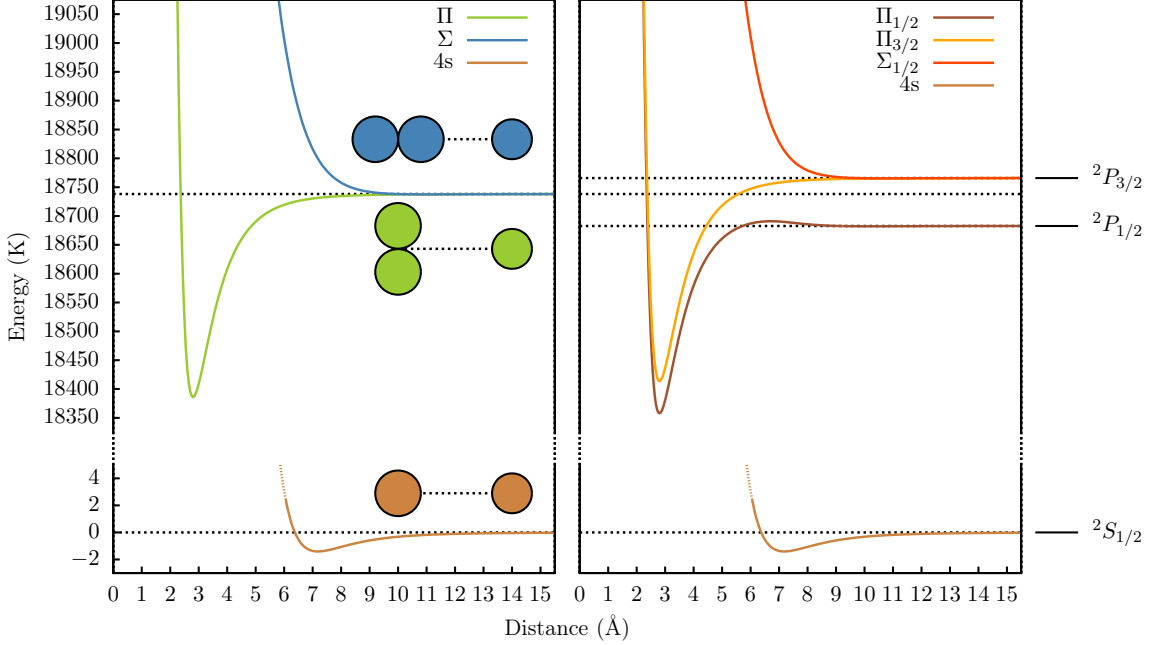


FIG. 5: He-K pair potentials, for K in its ground (4s) or first excited (4p) electronic state. Left plot: without spin-orbit interaction, showing the different curves depending on the orientation Π or Σ of the p electronic orbital relative to the internuclear axis. Right plot: with spin-orbit interaction, showing the splitting of the Π curve into $\Pi_{1/2}$ and $\Pi_{3/2}$ (see appendix D for notations). Note that the $\Pi_{3/2}$ curve is parallel to the initial (spinless) Π curve, while the $\Pi_{1/2}$ and $\Sigma_{1/2}$ curves are a result of the mixing of the Π and Σ curves by the spin-orbit interaction. (by courtesy of Maxime Martinez).

where R_n is the rotation that transforms the unit vector $\hat{\mathbf{z}}$ into the unit vector $\hat{\mathbf{r}}'_n$ ($z'_n // \hat{\mathbf{r}}'_n$).

For a system of N helium atoms and an excited impurity in a P state, the total interaction potential is built using the DIM model⁵

$$H^{DIM} = \sum_{n=1}^N \left\{ V_\Pi(r'_n) \mathbf{I} + [V_\Sigma(r'_n) - V_\Pi(r'_n)] R_n |p_{z'_n}\rangle \langle p_{z'_n}| R_n^{-1} \right\}, \quad (46)$$

where R_n is the rotation that transforms the unit vector $\hat{\mathbf{z}}$ of the common frame into the unit $\hat{\mathbf{r}}'_n$ vector parallel to the He _{n} -I axis for the n^{th} He atom. A schematic view of the impurity-helium droplet system is displayed in Fig. 6. It can be shown that in cartesian coordinates

$$\langle p_i | R_n | p_{z'_n} \rangle \langle p_{z'_n} | R_n^{-1} | p_j \rangle = \frac{r'_{in} r'_{jn}}{r'^2_n}, \quad (47)$$

where $r'_{1n} = x'_n$, $r'_{2n} = y'_n$, $r'_{3n} = z'_n$, and $r'^2_n = x'^2_n + y'^2_n + z'^2_n$. Thus, the matrix elements

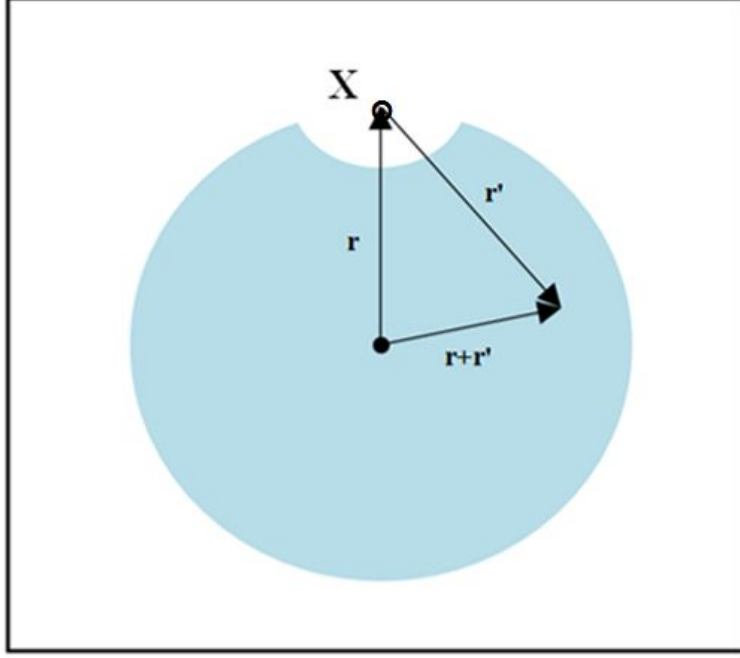


FIG. 6: Schematic figure displaying the X @ ${}^4\text{He}_N$ system and the coordinates used in the calculation of the X- ${}^4\text{He}_N$ interaction potentials (by courtesy of Albert Barranco).

of U are

$$\langle p_i | U | p_j \rangle \equiv U_{ij} = V_\Pi(r'_n) \delta_{ij} + [V_\Sigma(r'_n) - V_\Pi(r'_n)] \frac{r'_{ni} r'_{nj}}{r'^2_n}, \quad (48)$$

and the ones for the total droplet-I interaction in Eq. 46 are

$$\langle p_i | H^{DIM} | p_j \rangle \equiv H_{ij}^{DIM} = \sum_{n=1}^N \left\{ V_\Pi(r'_n) \delta_{ij} + [V_\Sigma(r'_n) - V_\Pi(r'_n)] \frac{r'_{ni} r'_{nj}}{r'^2_n} \right\}. \quad (49)$$

Using the continuous density approach inherent to DFT [$\sum_n \rightarrow \int d^3\mathbf{r}'' \rho(\mathbf{r}'')$], this expression can be written as

$$H_{ij}^{DIM}(\mathbf{r}_I) = \int d^3\mathbf{r}' \rho(\mathbf{r}' + \mathbf{r}_I) \left\{ V_\Pi(r') \delta_{ij} + [V_\Sigma(r') - V_\Pi(r')] \frac{r'_i r'_j}{r'^2} \right\}. \quad (50)$$

The eigenvalues $V_m^P(\mathbf{r}_I)$ of this symmetric matrix define the potential energy surfaces (PES) as a function of the distance between the center of mass of the droplet and that of the impurity. In the case of cylindrical symmetry, 2 of the eigenvalues are degenerate. In the case of spherical symmetry (*e.g.*, impurity at the center of the droplet), the three eigenvalues $V_m^P(\mathbf{r}_I)$ are degenerate.

The eigenvalues $V_m^P(\mathbf{r}_I)$ of H^{DIM} in Eq. (50) are given by the real roots $\lambda_i(\mathbf{r}_I)$ of the equation

$$\xi^3 + C\xi^2 + B\xi + A = 0 \quad (51)$$

with

$$\begin{aligned} C &= -\sum_{i=1}^3 H_{ii}^{DIM} \\ B &= \frac{1}{2} \sum_{i \neq j}^3 (H_{ii}^{DIM} H_{jj}^{DIM} - (H_{ij}^{DIM})^2) \\ A &= \sum_{i \neq j \neq k}^3 \left(\frac{1}{2} H_{ii}^{DIM} (H_{jk}^{DIM})^2 - \frac{1}{3} H_{ii}^{DIM} H_{jj}^{DIM} H_{kk}^{DIM} - \frac{2}{3} H_{ij}^{DIM} H_{jk}^{DIM} H_{ki}^{DIM} \right) \end{aligned} \quad (52)$$

It can be shown that for cylindrical geometry, Eq. (50) is diagonal with matrix elements (in spherical coordinates)

$$\begin{aligned} \xi_i(r_I) \equiv H_{ii}^{DIM}(r_I) &= 2\pi \int \int r'^2 \sin \theta' d\theta' dr' \rho(\sqrt{r'^2 + r_I^2 + 2r'r_I \cos \theta'}) \\ &\times \left\{ V_\Pi(r') + [V_\Sigma(r') - V_\Pi(r')] \left[\frac{1}{2}(\delta_{i1} + \delta_{i2}) \sin^2 \theta' + \delta_{i3} \cos^2 \theta' \right] \right\} \end{aligned} \quad (53)$$

In the case of spherical symmetry ($r_I = 0$ for a droplet at equilibrium, or bulk liquid at equilibrium for instance) integration over θ' can be performed and it is obtained:

$$\xi_i(r_I) \equiv H_{ii}^{DIM}(r_I = 0) = \frac{4\pi}{3} \int r'^2 dr' \rho(r') [V_\Sigma(r') + 2V_\Pi(r')] [\delta_{i1} + \delta_{i2} + \delta_{i3}] \quad (54)$$

which can be useful for tests.

When the spin-orbit (SO) interaction of the atomic impurity is negligible, e.g. for alkaline earth atoms, it can be safely neglected in the PES calculation. On the other hand, when it is comparable to the splitting of the P states due to the interaction with the droplet, it has to be taken into account in the calculation of the PESs. The total helium-impurity interaction can be written as $H^{\text{He}-I} = H^{DIM} + H^{SO}$, in which the spin-orbit coupling H^{SO} is approximated by that of the isolated atom

$$H^{SO} = A_{\ell s} \mathbf{L} \cdot \mathbf{S} = \frac{A_{\ell s}}{2} (\mathbf{J}^2 - \mathbf{L}^2 - \mathbf{S}^2) \quad \text{with} \quad \mathbf{J} = \mathbf{L} + \mathbf{S} \quad (55)$$

where \mathbf{L} and \mathbf{S} are the dopant electronic orbital and spin angular momenta, and \mathbf{J} the total electronic angular momentum. The value of the coupling constant $A_{\ell s}$ is deduced from the

spin-orbit splitting between the levels of the isolated atom. Here with $L = 1$ and $S = 1/2$, J can be either $3/2$ or $1/2$ and $A_{\ell s}$ is $2/3$ of the experimental splitting between these two levels. The previous cartesian orbital basis set is doubled by adding an index for the spin state $s = \uparrow$ ($m_s = 1/2$), $s = \downarrow$ ($m_s = -1/2$). In this basis $|p_x, \uparrow\rangle, |p_x, \downarrow\rangle, |p_y, \uparrow\rangle, |p_y, \downarrow\rangle, |p_z, \uparrow\rangle, |p_z, \downarrow\rangle$, H^{SO} is then given by

$$H^{SO} = \frac{A_{\ell s}}{2} \begin{pmatrix} 0 & 0 & -i & 0 & 0 & 1 \\ 0 & 0 & 0 & i & -1 & 0 \\ i & 0 & 0 & 0 & 0 & -i \\ 0 & -i & 0 & 0 & -i & 0 \\ 0 & -1 & 0 & i & 0 & 0 \\ 1 & 0 & i & 0 & 0 & 0 \end{pmatrix}. \quad (56)$$

In the same basis set, the matrix elements of U are

$$U_{ijss'}(\mathbf{r}') = \left[V_{\Pi}(r')\delta_{ij} + (V_{\Sigma}(r') - V_{\Pi}(r')) \frac{r'_i r'_j}{r'^2} \right] \delta_{ss'} \quad (57)$$

[compare with Eq. (48)].

Hence the total electronic Hamiltonian for a dopant in a P excited electronic state interacting with a helium droplet, $H^{\text{He}-I} = H^{\text{DIM}} + H^{SO}$, is a 6×6 matrix in the same basis set, with elements

$$H_{ijss'}^{\text{He}-I}(\mathbf{r}_I) = \delta_{ss'} \int d\mathbf{r}' \rho(\mathbf{r}') U_{ij}(\mathbf{r}' - \mathbf{r}_I) + H_{ijss'}^{SO} \quad (58)$$

Kramers' theorem states that for a total half integer spin value all levels are doubly degenerate and this degeneracy cannot be lifted by electrostatic interactions.⁴³ Hence the eigenstates of $H^{\text{He}-I}$ are two-fold degenerate. The PESs as a function of the distance between the impurity and the center of mass of the droplet are obtained as the (doubly degenerate) eigenvalues $\mathcal{V}_m^{2P}(\mathbf{r}_I)$ of $H^{\text{He}-I}$.

The eigenvalues $\mathcal{V}_m^{2P}(\mathbf{r}_I)$ of $H^{\text{He}-I}$ are the roots of the equation

$$\xi^3 + C\xi^2 + [B - \frac{3}{4}A_{\ell s}^2]\xi + \{A + \frac{1}{4}[A_{\ell s}^3 - A_{\ell s}^2C]\} = 0 \quad (59)$$

with A , B and C defined in Eq. (52). In the case of cylindrical geometry, the eigenvalues adopt a simple expression: [note that H^{DIM} with only 2 indices

refer to its 3×3 matrix given in Eq. (49)]

$$\begin{aligned}
\xi_1(\mathbf{r}_I) &= \frac{1}{2}(H_{11}^{DIM} + H_{33}^{DIM}) \\
&+ \frac{1}{4} \left[-A_{\ell s} + \sqrt{9A_{\ell s}^2 - 4A_{\ell s}(H_{11}^{DIM} - H_{33}^{DIM}) + 4(H_{11}^{DIM} - H_{33}^{DIM})^2} \right] \\
\xi_2(\mathbf{r}_I) &= H_{11}^{DIM} + \frac{A_{\ell s}}{2} \\
\xi_3(\mathbf{r}_I) &= \frac{1}{2}(H_{11}^{DIM} + H_{33}^{DIM}) \\
&+ \frac{1}{4} \left[-A_{\ell s} - \sqrt{9A_{\ell s}^2 - 4A_{\ell s}(H_{11}^{DIM} - H_{33}^{DIM}) + 4(H_{11}^{DIM} - H_{33}^{DIM})^2} \right]
\end{aligned} \tag{60}$$

They further simplify in the case of spherical symmetry to

$$\begin{aligned}
\xi_1(\mathbf{r}_I) &= H_{11}^{DIM} + \frac{1}{2}A_{\ell s} = \xi_2(\mathbf{r}_I) \\
\xi_3(\mathbf{r}_I) &= H_{11}^{DIM} - A_{\ell s}
\end{aligned} \tag{61}$$

This is the same as the spin-orbit eigenstates of the atom, with an added term representing the effect of the impurity-helium interaction.

The method has been extended in Ref. 44 to the case in which the impurity is in a D state.

The dynamic evolution of the electronic excited state of the impurity is described by introducing an additional degree of freedom, a six-component vector $|\lambda\rangle$, which describes the coefficients of the electronic state in the $|p_i, s\rangle$ basis introduced for H^{SO}

$$|\lambda\rangle = \sum_{is} \lambda_{is}(t) |p_i, s\rangle . \tag{62}$$

The vector is normalized: $|\langle \lambda | \lambda \rangle|^2 = 1$.

The complete set of dynamical variables characterizing the system thus consists of a complex effective wavefunction for helium $\Psi(\mathbf{r}, t)$ such that $\rho(\mathbf{r}, t) = |\Psi(\mathbf{r}, t)|^2$, a vector position for the impurity, $\mathbf{r}_I(t)$, and a 6-dimensional complex vector for its electronic state $|\lambda(t)\rangle$. In the following, the t -dependence of the dynamical variables is omitted to simplify the notation. The total energy of the $\text{I}@\text{He}_N$ complex in the 2P manifold is written as

$$E[\Psi, \mathbf{r}_I, \lambda] = \int d\mathbf{r} \frac{\hbar^2}{2m} |\nabla_{\mathbf{r}} \Psi|^2 + \frac{p_I^2}{2m_I} + \int d\mathbf{r} \mathcal{E}_c[\rho] + \langle \lambda | H^{SO} | \lambda \rangle + \int d\mathbf{r} \rho(\mathbf{r}) V_{\lambda}(\mathbf{r} - \mathbf{r}_I) . \tag{63}$$

In the above equation

$$V_\lambda(\mathbf{r}') \equiv \langle \lambda | U(\mathbf{r}') | \lambda \rangle = \sum_{ijss'} \lambda_{is}^* U_{ijss'}(\mathbf{r}') \lambda_{js'} , \quad (64)$$

where the six-dimensional matrix elements of U are given in Eq. (57).

The dynamical evolution is obtained from the variation of the action

$$\mathcal{A}[\Psi, \mathbf{r}_I, \lambda] = \int dt \left\{ E[\Psi, \mathbf{r}_I, \lambda] - i\hbar \int d\mathbf{r} \Psi^*(\mathbf{r}) \frac{\partial}{\partial t} \Psi(\mathbf{r}) - i\hbar \langle \lambda | \frac{\partial}{\partial t} | \lambda \rangle - \frac{1}{2} m_I \dot{\mathbf{r}}_I^2 \right\} \quad (65)$$

This yields three coupled equations

$$i\hbar \frac{\partial}{\partial t} \Psi = \left[-\frac{\hbar^2}{2m} \nabla_{\mathbf{r}}^2 + \frac{\delta \mathcal{E}_c}{\delta \rho(\mathbf{r})} + V_\lambda(\mathbf{r} - \mathbf{r}_I) \right] \Psi \quad (66a)$$

$$i\hbar \frac{\partial}{\partial t} | \lambda \rangle = H^{\text{He-}I} | \lambda \rangle \quad (66b)$$

$$m_I \ddot{\mathbf{r}}_I = -\nabla_{\mathbf{r}_I} \left[\int d\mathbf{r} \rho(\mathbf{r}) V_\lambda(\mathbf{r} - \mathbf{r}_I) \right] = - \int d\mathbf{r} V_\lambda(\mathbf{r} - \mathbf{r}_I) \nabla_{\mathbf{r}} \rho(\mathbf{r}) \quad (66c)$$

where Note also that Eq.(66b) for $| \lambda \rangle$ is a matrix equation, since $| \lambda \rangle$ is a 6-component vector. Note that if the impurity is treated as a classical particle, it does not have to remain inside the calculation box during all the simulation. This is only required for the droplet, in order to calculate the acceleration of the impurity [see the right-hand of Eq. (66c)].

C. Initial conditions

In order to solve the sets of equations such as Eqs. (41), Eqs. (43) or Eqs. (66), initial values for the variables are required. Their choice is guided by the physics of the process. The helium order parameter and the location of the impurity are taken as the solution of the static problem. The initial value for the impurity velocity is taken as zero for photoexcitation or photoionization, or as the experimental value for collisions. There remains to fix the initial $| \lambda \rangle$ state. In the case of a photon-induced process this is usually done, somewhat arbitrarily, by choosing one of the eigenstates with energy $\mathcal{V}_m^{2P}(\mathbf{r}_I)$ resulting from the diagonalization of the Hamiltonian $H^{\text{He-}I}$ [Eqs. (58)-(61)] (or $V_m^P(\mathbf{r}_I)$ from H^{DIM} [Eqs. (50)-(54)] in the case where spin-orbit coupling can be neglected) at the time of excitation or ionization. It is equivalent to assuming that the light pulse is long enough to excite only one of the eigenstates

of the system, while short enough that the nuclei do not have time to move. However, there are other possibilities that will be described below, as for instance the electronic configuration corresponding to an impurity-helium exciplex (see Section V page 41). For a collision, the initial $|\lambda\rangle$ state is usually the ground electronic state of the isolated impurity.

For most helium distributions considered, the dominant term in the electronic Hamiltonian Eq. (58) in the Franck-Condon region is the spin-orbit interaction H^{SO} . Hence, depending on the value one finds for the expectation value $\langle H^{SO} \rangle$ on these eigenstates they can be arranged into two sets, one consisting of a doublet that correlates to the atomic $J = 1/2$ doublet, and another set consisting of two doublets that correlate to the atomic $J = 3/2$ quartet. Accordingly, the evolution corresponding to the $|^2\Pi_{1/2}\rangle$ state is initiated with one of the eigenstates of the doublet correlated to the $J = 1/2$ manifold. In order to select one of the other two states as the initial state, we have diagonalized the J_z operator in the mentioned fourfold vector space. This results in a doublet with $\Omega = \pm 3/2$ and another one with $\Omega = \pm 1/2$. Either member of the former doublet can be used to start the evolution corresponding to the $|^2\Pi_{3/2}\rangle$ state, and either of the latter can be used to start the evolution corresponding to the $|^2\Sigma_{1/2}\rangle$ state.

D. Technical details on how the dynamic equations are solved

Equations (41), (43), or (66) are usually solved within the same box and using the same grid as for the static problem. The time step employed is about 0.5 fs in most applications. We use Hamming's predictor-modifier-corrector method as explained in chapter 8 of Ref. 45. An introductory description of the predictor-corrector and Runge-Kutta methods can be found in Ref. 32. The presentation of both approaches in Ref. 45 is particularly clear and useful.

Let us briefly indicate here the basic equations of Hamming's predictor-modifier-corrector method . In general one aims at integrating a system of N ordinary differential equations

$$\frac{dy}{dx} = f(x, y) \quad (67)$$

with the initial conditions $y(x_0) = y_0$, where y and f are N -component vectors. Higher order differential equations can be reduced to a system of first order

equations. For instance, Eq. (66c) can be written as

$$\begin{aligned}\frac{d\mathbf{r}_I}{dt} &= \mathbf{v}_I \\ \frac{d\mathbf{v}_I}{dt} &= -\frac{1}{m_I} \int d\mathbf{r} V_\lambda(\mathbf{r} - \mathbf{r}_I) \nabla_{\mathbf{r}} \rho(\mathbf{r})\end{aligned}\quad (68)$$

The solution of the system of Eqs. (66) is obtained through the following steps [see Eqs. (21) in chapter 8 of Ref. 45]:

$$\begin{aligned}\text{Predictor : } p_{n+1} &= y_{n-3} + \frac{4h}{3}[2y'_n - y'_{n-1} + 2y'_{n-2}] \\ \text{Modifier : } m_{n+1} &= p_{n+1} - \frac{112}{121}[p_n - c_n] \\ m'_{n+1} &= f(x_{n+1}, m_{n+1}) \\ \text{Corrector : } c_{n+1} &= \frac{1}{8}[9y_n - y_{n-2} + 3h(m'_{n+1} + 2y'_n - y'_{n-1})] \\ \text{Final value : } y_{n+1} &= c_{n+1} + \frac{9}{121}[p_{n+1} - c_{n+1}]\end{aligned}\quad (69)$$

The error of the scheme is $\mathcal{O}(h^5)$.

One of the advantages of the method is that it only requires the calculation of two values of $f(x, y)$ per step h . In our case, evaluating the mean field is the most time-consuming part of the iteration procedure, which is why this method is preferred to others such as the very popular Runge-Kutta method.³² On the other hand, it requires to store two previous values of f and three previous values of y , but it is not a limitation in our case since the number of components of y is small.

Hamming's method is not self-starting as can be seen in Eqs. (69), since it requires the values of the solution at three preceding steps. These starting values should be evaluated with an accuracy at least as high as the one of the Hamming's method; otherwise, large errors in the first few steps could degrade the overall accuracy or even make the whole procedure unstable. In our case, the first time steps are obtained by a Runge-Kutta-Gill method as described in chapter 9 of Ref. 45:

$$\begin{aligned}k_1 &= hf(x_0, y_0) \\ y_1 &= y_0 + \frac{1}{2}(k_1 - 2q_0) \\ q_1 &= q_0 + \frac{3}{2}(k_1 - 2q_0) - \frac{1}{2}k_1 \\ k_2 &= hf\left(x_0 + \frac{h}{2}, y_1\right) \\ y_2 &= y_1 + (1 - \sqrt{1/2})(k_2 - q_1) \\ q_2 &= q_1 + 3(1 - \sqrt{1/2})(k_2 - q_1) - (1 - \sqrt{1/2})k_2\end{aligned}$$

$$\begin{aligned}
k_3 &= hf \left(x_0 + \frac{h}{2}, y_2 \right) \\
y_3 &= y_2 + (1 + \sqrt{1/2})(k_3 - q_2) \\
q_3 &= q_2 + 3(1 + \sqrt{1/2})(k_3 - q_2) - (1 + \sqrt{1/2})k_3 \\
k_4 &= hf(x_0 + h, y_3) \\
y_4 &= y_3 + \frac{1}{6}(k_4 - 2q_3) \\
q_4 &= q_3 + \frac{1}{2}(k_4 - 2q_3) - \frac{1}{2}k_4 \\
y(x_0 + h) &= y_4 + \mathcal{O}(h^5)
\end{aligned} \tag{70}$$

To go from x_0 to $x_0 + h$ in the first step one takes $q_0 = 0$; in the next steps, q_0 is set to the q_4 value of the previous one (that is not zero due to roundoff errors). Note that the Runge-Kutta method requires four evaluations of f per step h . A final word of caution: the starting method should at least be of the same order [$\mathcal{O}(h^5)$ in this case] than that used for the rest of the time propagation.

E. Absorbing potential at the box boundaries

During the time evolution of excited impurities in bulk liquid helium, sound waves are released from the surface of the atomic bubble and eventually reach the cell boundary. If no action is taken, they will bounce back and spoil the simulation. In the case of doped droplets, this can also happen when some helium is ejected off the droplet in the course of the dynamics. In this case, particle –and thus energy– leaking appears when some helium density gets near the walls of the calculation box. This leaking is physical, it represents helium atoms leaving the droplet and the energy carried away by them. This material also has to be prevented from bouncing back.

A way to prevent this problem is to include some damping (absorption potential) into the time-dependent equation governing the helium evolution, as *e.g.* Eq. (66a).

We make the replacement $i \rightarrow i + \Lambda(\mathbf{r})$ into the dynamic equation of the helium.²⁰ This corresponds to a rotation of the time axis in the complex plane by introducing a damping field $\Lambda(\mathbf{r})$. This is equivalent to adding a purely imaginary potential $i\Lambda(\mathbf{r})$ which has the effect of absorbing helium density in the region where it is non zero. $\Lambda(\mathbf{r})$ is taken as

$$\Lambda(\mathbf{r}) = \Lambda_0 \left[1 + \tanh \left(\frac{s - s_0}{a} \right) \right], \quad s \equiv |\mathbf{r}|. \tag{71}$$

We have fixed $\Lambda_0 = 2$ and $a = 2$ in “internal use” units (see Appendix B page 51). The evolution is damping-free [$\Lambda(\mathbf{r}) \ll 1$] in a sphere of radius $s < s_0 - 2a$.

The region in which the absorption potential acts has to be large enough to accommodate the part of the system under study, and can be geometry-adapted. This means that absorption can be made to act only on the cell boundaries that are expected to be hit by the “evaporated” helium atoms (top boundary, lateral boundaries, all boundaries, …). If for instance we just include absorption in the z direction, Eq. (71) reduces to

$$\Lambda(z) = \Lambda_0 \left[1 + \tanh\left(\frac{|z| - s_0}{a}\right) \right]. \quad (72)$$

The value of s_0 is taken to be 2-3 Å less than the maximum $|z|$ value in the calculation box.

The above prescription works extremely well, as it efficiently dampens the excitations of the helium wave function at the cell boundaries in the case of extended systems, or absorbs the helium atoms leaving the simulation box in the case of droplets. Moreover, it does not require a large buffer region —actually we use the same box as the one for static calculations.

If the impurity is treated classically, its motion can be followed irrespective of whether it is inside or outside the simulation box. The same happens if its quantal evolution is described by test particles, as explained in section VI. If the impurity dynamics was described by a wave packet —which we have not done so far— one should also take care of the reflection of the wave packet at the cell boundaries. This could be done by the trick just described, which is commonly used in wave packet propagation where it is called “optical” or “absorbing potential” or “absorbing boundary conditions” method.^{46,47}

Finally, we mention that for the method to work in the bulk liquid, the –known– chemical potential of the helium must be included in the TDDFT evolution equation, see Eq. (4) of Ref. 20.

IV. ABSORPTION AND EMISSION SPECTRUM WITHIN THE DF SAMPLING METHOD

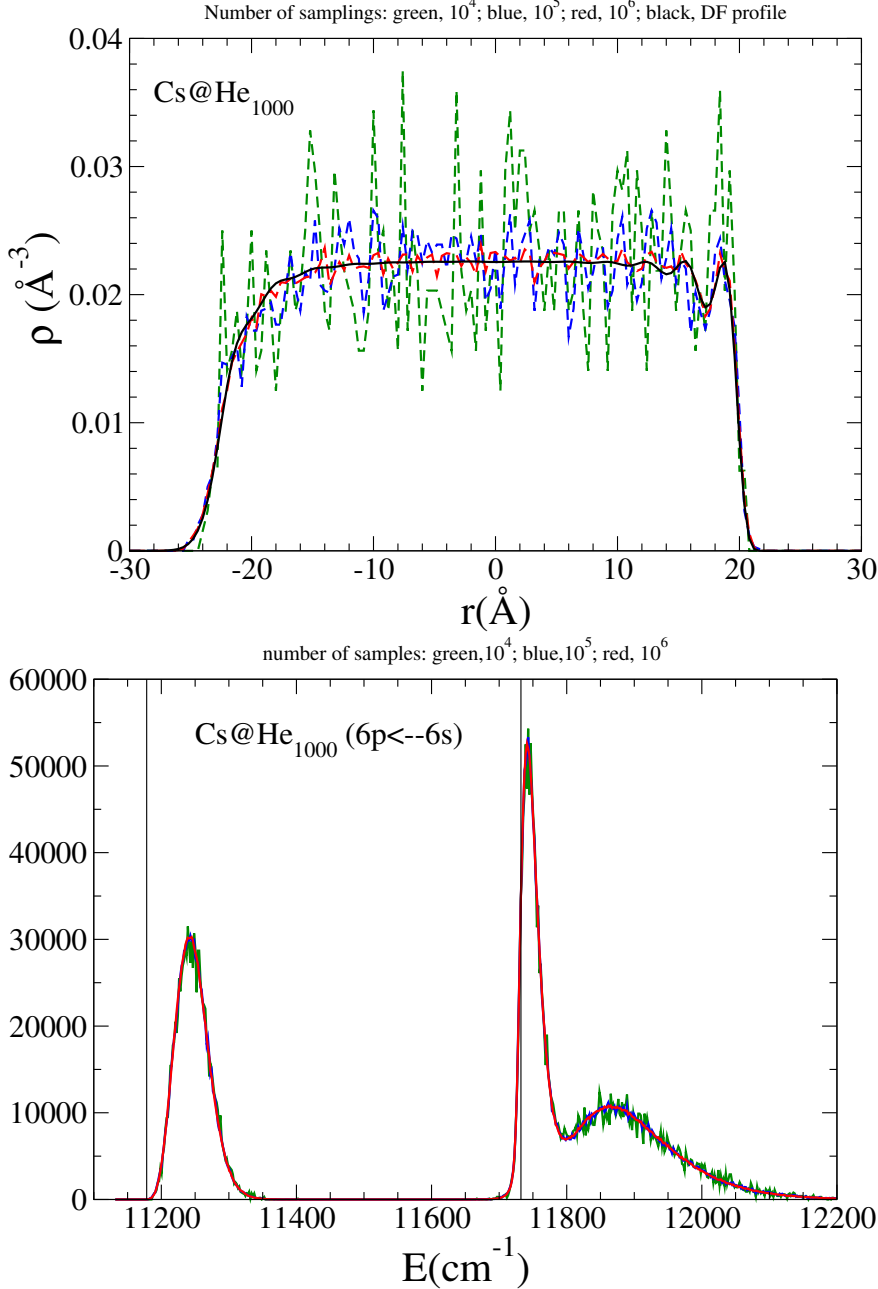


FIG. 7: Top figurel: DFT density profile along the z axis [$\rho(z)$] of the Cs@ ${}^4\text{He}_{1000}$ droplet (solid line) and the simulated profile corresponding to $n_c = 10^4$, 10^5 , and 10^6 simulations. Bottom figure: $6p \leftarrow 6s$ absorption spectrum of Cs obtained using the corresponding sampled density distribution. We have used Patil's He-Cs potential⁴⁸ for the ground state and Pascale's He-Cs potentials⁴⁹ for the excited states. The spectrum is given in arbitrary units and in the case of $n_c = 10^4$ and 10^5 it has been multiplied by a factor of 100 and 10 respectively so that they can be compared to that of $n_c = 10^6$

A. Absorption

The dipolar absorption spectrum of the dopant-droplet system is one of the key observables to be addressed. Comparing it with that of the dopant in bulk liquid helium was used in the past to ascertain whether the dopant resides in the bulk or at the droplet surface, see *e.g.* Ref. 50. Besides, comparing it to experiment is a stringent test on the accuracy of the ingredients of the simulation (density distributions, pair potentials, …), which should be carried out before any dynamic evolution triggered by the photoexcitation of the impurity. Within the scheme described by Eqs. (44-61), the absorption peaks are the eigenvalues $\mathcal{V}_m^{2P}(\mathbf{r}_I)$ of $H^{\text{He}-I}$ [Eqs. (58-61)], or of the eigenvalues $V_m^P(\mathbf{r}_I)$ of H^{DIM} [Eqs. (50-54)] if spin-orbit coupling can be neglected, \mathbf{r}_I being the equilibrium location of the impurity in the ground electronic state denoted by X . The width of the absorption spectrum comes from fluctuations in the helium density⁵¹ and/or from the probability distribution $|\phi^i(\mathbf{r}_I)|^2$ of \mathbf{r}_I if the impurity is treated quantum mechanically.⁵² To incorporate the density fluctuations, we use the DF sampling method described in detail in Ref. 51. We discuss it here for the sake of completeness.

Within the framework of the Born-Oppenheimer approximation, the electronic and nuclear wave functions can be factorized. Using the time-dependent formulation,⁴ the line shape for an electronic transition from the initial (ground) i to the final (excited) f electronic state is obtained as the Fourier transform of the time-correlation function

$$I(\omega) \propto \sum_m \int dt e^{i(\omega+\omega^i)t} \int d^3\mathbf{r}_I \Phi^{i*} e^{(-it/\hbar)H_m^f} \Phi^i, \quad (73)$$

In this equation, $\Phi^i(\mathbf{r}_I) = \mu_{f \leftarrow i} \phi^i(\mathbf{r}_I)$ where $\phi^i(\mathbf{r}_I)$ is the eigenfunction of the impurity in the initial state with energy $\hbar\omega^i$; $\mu_{f \leftarrow i}$ the electronic transition dipole moment from i to f ; and H_m^f is the dopant Hamiltonian in the final state. It is written as $H_m^f = T_{kin} + V_m^f(\mathbf{r}_I)$, where T_{kin} is the kinetic energy operator and $V_m^f(\mathbf{r}_I)$ is the potential energy surface in the final state. For a single excited electronic state (*e.g.* S excited state for an atom) index m can be omitted. In the case of multiple electronic states, $V_m^f(\mathbf{r}_I)$ is the m^{th} eigenvalue of the excited potential matrix [$\mathcal{V}_m^{2P}(\mathbf{r}_I)$, Eq. (59-61), in the case of a P excited state including spin-orbit coupling]. In the studies done so far, $\mu_{f \leftarrow i}$ has been assumed to vary slowly with r_I and neglected (Franck-Condon approximation). $\phi^i(\mathbf{r})$ is then expanded in the basis set of

the eigenfunctions $\varphi_\nu^m(\mathbf{r})$ of H_m^f with energies $\hbar\omega_\nu^m$

$$\phi^i(\mathbf{r}) = \sum_\nu a_\nu^m \varphi_\nu^m(\mathbf{r}_I), \quad a_\nu^m = \int d^3\mathbf{r} \varphi_\nu^{m*}(\mathbf{r}_I) \phi^i(\mathbf{r}_I) \quad (74)$$

Introducing this expression in Eq. (73), we obtain

$$\begin{aligned} I(\omega) &\propto \sum_m \int dt e^{-i(\omega+\omega^i)t} \sum_\nu |a_\nu^m|^2 e^{i\omega_\nu^m t} \\ &= \sum_m \sum_\nu |a_\nu^m|^2 \delta[\omega - (\omega_\nu^m - \omega^i)], \end{aligned} \quad (75)$$

The spectrum is a series of lines at energies $\hbar(\omega_\nu^m - \omega^i)$ with relative intensities $|a_\nu^m|^2$. $|a_\nu^m|^2$ are called the Franck-Condon factors.

If the final states correspond to the continuous or quasi-continuous spectrum of H_m^f , it can be assumed that $\langle T_{kin} \rangle \ll \langle V_m^f \rangle$, and the Hamiltonian is approximated as $H_m^f \sim V_m^f(\mathbf{r})$. Introducing this approximation in Eq. (73) and integrating over time we get the semiclassical expression for $I(\omega)$, also called “reflection principle”⁵³, that we use to simulate absorption or emission spectra

$$I(\omega) \propto \sum_m \int d^3\mathbf{r}_I |\phi^i(\mathbf{r}_I)|^2 \delta [\omega - (V_m^f(\mathbf{r}_I)/\hbar - \omega^i)] . \quad (76)$$

This expression is evaluated as follows. Firstly, the helium distribution is stochastically represented by a large number of configurations n_c , of the order of 10^6 . Each configuration consists of a set of N positions for the He atoms in the simulation box, and one for the impurity. The helium positions are randomly generated by importance sampling techniques, using the helium density $\rho(\mathbf{r})/N$ as the probability density distribution, plus a hard-sphere repulsion between He atoms to approximately take into account He-He correlations. This is represented by an exclusion volume around the helium positions already sampled: if the next helium position falls within the exclusion volume around any of the already selected heliums, it is rejected and a new sample is done. The diameter of the exclusion sphere has to be of the order of $h = 2.18 \text{ \AA}$ in order to be consistent with the DF description of the liquid, since h is the length used in the functional to screen the Lennard-Jones interaction between particles and to compute the coarse grained density.²² We have chosen a density-dependent

sphere radius of the form

$$R_j = R(\mathbf{r}_j) = \frac{h}{2} \left(\frac{\rho_0}{\bar{\rho}(\mathbf{r}_j)} \right)^{1/3}, \quad (77)$$

around helium atom j at \mathbf{r}_j , where ρ_0 is the saturation density value and $\bar{\rho}$ is the coarse-grained density, defined as the averaged density over a sphere of radius h . Although this scaling has no effect in the bulk, it is essential to correctly reproduce the density in the droplet surface region. The rationale for choosing this form for R_j is sketched in the Appendix of Ref. 51.

If the impurity is treated quantum mechanically, its position is also randomly generated using $|\phi^i(\mathbf{r}_I)|^2$ as its probability density distribution. Otherwise only its equilibrium position in the i electronic state is used. We show in Fig. 7 the sampled density along the z axis compared with the DF density profile for several n_c values. The system is Cs@ ${}^4\text{He}_{1000}$. As an example for a light impurity treated quantum-mechanically, Fig. 8 shows the DF and sampled densities for Na@ ${}^4\text{He}_{1000}$ in a symmetry plane of the complex.⁵²

The line shape of the spectrum is obtained by collecting the transition energies of all the sampled configurations in a histogram. Specifically, for a given sampled configuration $\{k\}$ the transition energy is

$$E\{k\} = V_m^f\{k\} - V^i\{k\}, \quad (78)$$

where $V^i\{k\} = \sum_j V_{\text{He}-I}^i(|\mathbf{r}_j^{(k)} - \mathbf{r}_I^{(k)}|)$ is the sum of helium-dopant pairwise interactions in the initial state and $V_m^f\{k\}$ are the eigenvalues of the excited state interaction energy matrix $\sum_j U(|\mathbf{r}_j^{(k)} - \mathbf{r}_I^{(k)}|) + H^{SO}$ [Eq. (57) plus the SO interaction from Eq. (56)]. The histogram of the collected stochastic energies is identified with the absorption spectrum

$$I(\omega) \propto \sum_m \frac{1}{n_c} \sum_{\{k\}}^{n_e} \delta [\omega - (V_m^f\{k\} - V^i\{k\})/\hbar]. \quad (79)$$

In this way, we obtain the absorption spectrum of impurities in liquid helium including shape fluctuations.

Let us briefly indicate how the histogram is obtained. An educated guess is made for the energy interval (E_{\min}, E_{\max}) where the spectrum lies, and for the number of energy bins. This defines the histogram energy step Δ_E . The energy bin i where a particular excitation energy $E\{k\}$ [Eq. (78)] falls is determined

as

$$i = \text{Integer} \left[\frac{E\{k\} - E_{\min}}{\Delta_E} \right] + 1 \quad (80)$$

A unit is added to the i^{th} bin content every time an excitation energy $E\{k\}$ falls inside the bin. The histogram representing the spectrum is obtained by carrying out this procedure for the n_c configurations. The initial guess for the energy interval or for the number of bins has to be corrected if the overall aspect of the histogram is not satisfactory. If some of the lines are abruptly cut for instance, the energy interval is too narrow. A number of energy bins too small makes the spectrum too wiggly (too small a n_c value causes the same effect, see Fig. 7).

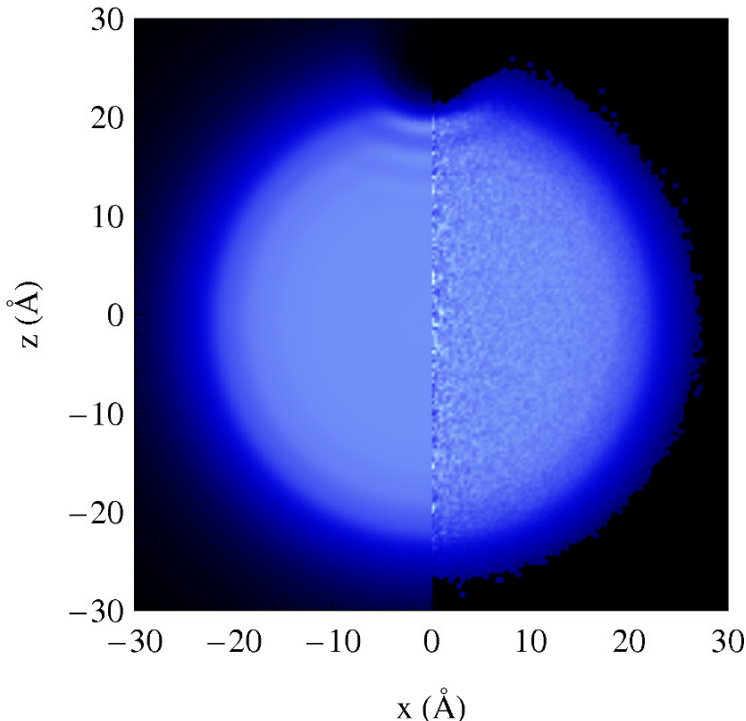


FIG. 8: Helium density corresponding to $\text{Na}@\text{He}_{1000}$ on a plane of symmetry of the complex.⁵² Left region: result of the DF calculation. Right region: simulated density using $n_c = 10^6$ configurations. The brighter the color, the higher the density.

It is worth mentioning that the absorption spectrum obtained this way is not normalized. Dividing by n_c in Eq. (79) is only necessary when checking for convergence of the histogram with respect to the number of sampled configurations n_c . We stress however, that the relative intensity of the peaks is properly described.

Usually the zero energy for the V_Σ and V_Π pair potentials is taken at their dissociation limit. The above expressions then yield the shift of the spectrum with respect to that of

the free atom. In order to compare with an experimental spectrum one has to add the absorption energy of the free-atom (only the term energy provided by *e.g.* NIST⁵⁴ since the spin-orbit interaction is included in the calculation)

Fig. 7 shows the absorption spectrum corresponding to the $6p \leftarrow 6s$ transition of Cs in a ${}^4\text{He}_{1000}$ droplet obtained using $n_c = 10^4, 10^5$, and 10^6 configurations for the sampled helium density. It is remarkable that in spite of the straggling in the $\rho(z)$ density profile, the line shape is well reproduced using a number of configurations as small as 10^5 .

Note that other sources of broadening such as thermal wandering⁴² or droplet size distribution effects may have some influence –especially for impurities sitting at the outer surface of the droplet– but are not accounted for by this procedure.

B. Emission

The emission spectrum is calculated in a similar way.⁴⁴ First, one has to obtain the helium density relaxed around an excited state. In the case of a single excited state the procedure is the same as for the ground state, using the excited state helium-dopant interaction potential instead of the ground state one. In the case of multiple excited states, the relaxed configuration for a given excited state $|\lambda\rangle$ of the dopant is obtained by solving the coupled equations

$$\left[-\frac{\hbar^2}{2m} \nabla^2 + \frac{\delta\mathcal{E}_c}{\delta\rho(\mathbf{r})} + V_\lambda(\mathbf{r}) \right] \Psi = \mu \Psi \quad (81\text{a})$$

$$H^{\text{He-}I} |\lambda\rangle = \epsilon_\lambda |\lambda\rangle , \quad (81\text{b})$$

where $V_\lambda(\mathbf{r})$ has been defined in Eq. (64) and $H^{\text{He-}I}$ in Eq. (58). The general case procedure to determine the relaxed configuration is

1. Start from the helium density corresponding to *e.g.* the configuration with the ground electronic state impurity at a given point of the droplet.
2. Determine the internal electronic states corresponding to that helium density by diagonalizing $H^{\text{He-}I}$ [Eq. (58)]. This yields three two-fold degenerate states $|\lambda\rangle$. Choose one of them and build the potential $V_\lambda(\mathbf{r})$, Eq. (64).
3. Using $V_\lambda(\mathbf{r})$, carry out a relaxation step as indicated by Eq. (81a) to determine the

new $\rho(\mathbf{r})$ and use it to update $H^{\text{He}-I}$. Then carry out a relaxation step (81b) to update $|\lambda\rangle$ and ϵ_λ . Iterate until μ and ϵ_λ converge

Upon convergence, the total energy of the droplet-impurity complex is given by Eq. (63) ($p_I = 0$). Changes to be made when the impurity is treated as a quantum particle are obvious and are not described here. They have not been implemented yet because of a technical limitation related to the fast Fourier transform of the in general non-spherical potential $V_\lambda(\mathbf{r})$, see especially Eq. (57).

The DF sampling method for calculating the spectrum is carried out for this density. The “final” state potential corresponds to the state to which the impurity is being de-excited (usually the ground electronic state), and the “initial” state is $|\lambda\rangle$, with potential V_λ determined above Eq. (64).

V. THE PARTICULAR CASE OF EXCIPLEXES

A. A molecular model of the exciplexes

It has appeared that some interesting impurity-droplet complexes are overlooked if one proceeds as explained in the previous sections. One such case is that of exciplexes, a kind of configurations in which some He atoms are attached to the impurity in an excited electronic state, whereas they are not when the impurity is in the ground state. The formation of a linear, $^2\Pi_{3/2}$ exciplex around the $^2P_{3/2}$ electronic excited state of impurities such as Ag⁴¹ and Ba⁺⁴⁴ could be described within the TDDFT dynamics because it is a barrierless process. However, in many other cases the formation of exciplex configurations is hindered by an energy barrier that prevents them from being found by the imaginary time minimization procedure.

We show here how to find other exciplex configurations, such as those around the $^2P_{1/2}$ (*i.e.* $^2\Pi_{1/2}$ for the linear complex) state of some impurities. We take Ba⁺ as a case of study. Electronic excitation of Ba⁺ creates a “bubble” configuration in which helium is distributed around the impurity leaving an empty space around the cation. Quantum diffusion Monte Carlo simulations⁵⁵ of He₂Ba⁺($^2\Pi_{1/2}$) complexes have determined a nearly linear geometry with Ba⁺ between the two He atoms, each at some 3 Å from the cation. This distance is significantly smaller than the radius of the excited cation bubble. The bubble configuration and the linear exciplex configurations are separated by an energy barrier that cannot be overcome by the TDDFT dynamics. Also shown in Ref. 55 are ring-like He_nBa⁺($^2\Pi_{1/2}$) configurations with up to $n = 7$ He atoms, the largest number of He atoms considered there.

Interestingly, linear and ring Cs*He_n exciplexes were also found in solid helium⁵⁶ and discussed within a model that can be straightforwardly applied to other impurities. Being far simpler than DFT and DMC approaches while realistic enough, this model is a useful guide for implementing the search of exciplexes within DFT.

Following Ref. 56, the interaction between one Ba⁺ cation and n He atoms is described as indicated by Eq. (58), fixing the origin of coordinates at the cation location and replacing the integral over He density by a sum over the He atoms. For the linear $n = 2$ configuration, both He atoms are axially located at a distance r on opposite sides of the Ba⁺ cation. For the $n > 2$ ring configurations the He atoms are evenly distributed along a ring of radius r

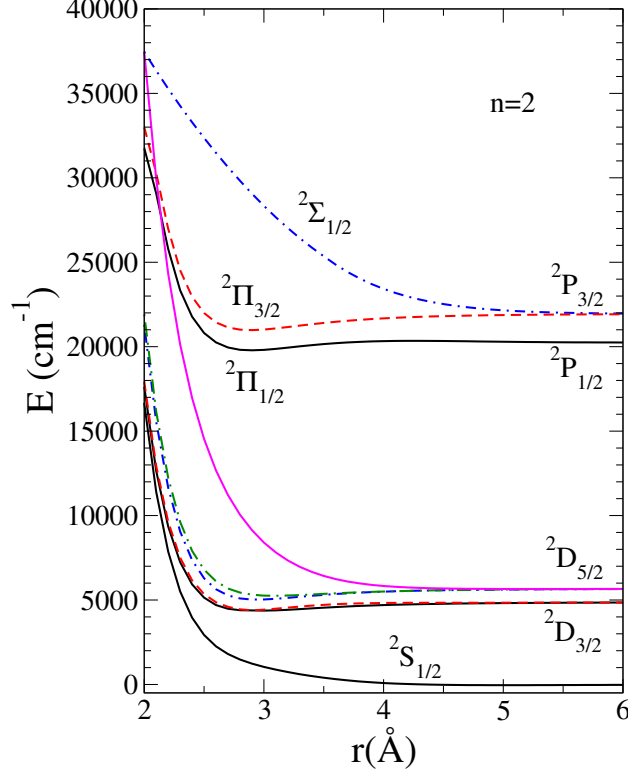


FIG. 9: $\text{Ba}^+(\text{2}\Pi_{1/2})\text{He}_2$ PES as a function of the distance r between each He atom and the Ba^+ cation. Also displayed are the energies of the ^2S and ^2D PES obtained for this linear configuration.

centered at the cation. The total He-He energy is then added to the cation-He interaction as a sum of pair interactions. The He-He interaction is taken as the screened Lennard-Jones potential that enters the definition of the Orsay-Trento functional. The results presented below are sensibly the same if the He-He Aziz potential⁵⁷ is used. Adding the spin-orbit interaction, one obtains the total energy of the complex as a function of r . The model assumes that the remaining He atoms in the droplet do not affect the local structure of the exciplex around the Ba^+ cation.

Diagonalizing the total energy for a given n as a function of r yields the potential energy surfaces (PES) that correlate with the He- $\text{Ba}^+(\text{2}P_{3/2})$ and $(^2\text{P}_{1/2})$ potentials at long distances. Fig. 9 displays the PES for $n = 2$, showing the appearance of a linear exciplex around the $^2\text{Pi}_{1/2}$ state of Ba^+ at $r \sim 3 \text{ \AA}$. Ring exciplexes have been also found.⁴⁴

B. Exciplex formation within static and time-dependent DFT

Diagonalizing the energy within the previous molecular model does not only give the impurity-helium distance of the linear (or ring) exciplex configuration. It also gives the eigenvector $|\lambda\rangle$ corresponding to an electronic state of the impurity in the exciplex. This $|\lambda\rangle$ state can be used as an initial choice to start the dynamics or the static relaxation process⁴⁴ when the method outlined in section IV B does not lead to an exciplex because of an energy barrier preventing its formation from the bubble configuration.

In this case, the starting electronic state is taken as an eigenvector $|\lambda\rangle$ corresponding to an electronic state of the impurity in the exciplex model from the previous section, instead of an eigenvector of $H^{\text{He}-I}$ as in section IV B. On the other hand, the starting helium density is still taken as the helium density corresponding to the configuration with the ground electronic state impurity at a given point of the droplet, as in section IV B. Upon DFT relaxation of both the helium density and the electronic state, the chosen exciplex is obtained,⁴⁴ and it persists even in the presence of the rest of the helium atoms in the droplet. Indeed, it has been found to be fully contained inside the cation bubble.⁴⁴

Similarly, the TDDFT Eqs. (66) have also been found to lead to the *dynamic* formation of the exciplex configuration⁴⁴ when taking an initial electronic state $|\lambda\rangle$ corresponding to an exciplex in the model of Ref. 56.

VI. THE TEST-PARTICLE METHOD APPLIED TO THE SOLUTION OF THE SCHRÖDINGER EQUATION FOR THE IMPURITY

If the impurity-helium interaction is highly repulsive when the impurity is in an excited state, the impurity velocity can become very large. Inside the droplet this velocity eventually falls below the Landau critical velocity (~ 50 m/s) because the swift impurity excites elementary modes of the droplet, thus losing kinetic energy. This is not instantaneous, hence for a short period of time the impurity velocity can become very large. It can be even larger if the impurity leaves the droplet, in which case there is no mechanism to slow it down.

When the impurity is light it cannot be described as a classical particle and one has to resort to a quantum description. In this case the impurity wave function displays fast oscillations whose description would require a very fine mesh, making a 3D approach com-

putationally unaffordable since the same grid is used for the impurity and for the helium density. A possible way out, that has been successfully applied to the case of excited Li and Na impurities in helium droplets,⁴⁰ is to simulate the solution of the Schrödinger equation for the impurity using test particles (Bohmian dynamics³⁹). We describe in the following the basics of the method.

Our goal is to solve Eq. (43b), that is schematically written as follows

$$i\hbar \frac{\partial}{\partial t} \phi(\mathbf{r}_I, t) = \left[-\frac{\hbar^2}{2m_I} \nabla_{\mathbf{r}_I}^2 + V(\mathbf{r}_I) \right] \phi(\mathbf{r}_I, t) . \quad (82)$$

The complex wave function is written as

$$\phi(\mathbf{r}_I, t) \equiv \varphi(\mathbf{r}_I, t) e^{i\mathcal{S}(\mathbf{r}_I, t)} , \quad (83)$$

where φ and \mathcal{S} are *real* functions. Note that $|\phi|^2 = \varphi^2$. Moreover, it is assumed that $\varphi \geq 0$.³⁹ The usefulness of this decomposition is that while the real and imaginary parts of Φ may strongly oscillate in time, the density probability φ^2 and phase \mathcal{S} are much smoother functions of t .⁴⁰ Defining $\mathbf{v} \equiv (\hbar/m_I) \nabla_{\mathbf{r}_I} \mathcal{S}$, the current density $\mathbf{j}(\mathbf{r}_I, t) \equiv \hbar/(2m_I i) [\Phi^* \nabla_{\mathbf{r}_I} \Phi - \Phi \nabla_{\mathbf{r}_I} \Phi^*]$ becomes $\mathbf{j} = \varphi^2 \mathbf{v}$. Substituting Eq. (83) into Eq. (82) and equating the real and imaginary parts of the left and right hand terms one gets the equations in φ and \mathcal{S} :

$$\frac{\partial \varphi^2}{\partial t} = -\nabla_{\mathbf{r}_I} \cdot \mathbf{j} \quad [\text{continuity equation}] \quad (84a)$$

$$-\hbar \frac{\partial \mathcal{S}}{\partial t} = \frac{1}{2} m_I \mathbf{v}^2 + \mathcal{Q}(\mathbf{r}_I, t) + V \quad [\text{quantum Hamilton-Jacobi equation}] , \quad (84b)$$

where we have introduced the so-called quantum potential $\mathcal{Q}(\mathbf{r}_I, t)$:

$$\mathcal{Q}(\mathbf{r}_I, t) \equiv -\frac{\hbar^2}{2m_I} \frac{\nabla_{\mathbf{r}_I}^2 \varphi}{\varphi} \quad (85)$$

Equations (84) have been solved using test particles as follows. Writing the probability density and the current density at time t as a histogram of M test particles with trajectories

$\{\mathbf{R}_i(t)\}_{i=1}^M$, where $\mathbf{R}_i(t) = \mathbf{R}(\mathbf{r}_{Ii}, t)$ and $\mathbf{R}_i(0) = \mathbf{r}_{Ii}$, we get

$$\begin{aligned}\varphi^2(\mathbf{r}_I, t) &= \lim_{M \rightarrow \infty} \frac{1}{M} \sum_{i=1}^M \delta[\mathbf{r}_I - \mathbf{R}_i(t)] \\ \mathbf{j}(\mathbf{r}_I, t) &= \lim_{M \rightarrow \infty} \frac{1}{M} \sum_{i=1}^M \mathbf{v}[\mathbf{R}_i(t)] \delta[\mathbf{r}_I - \mathbf{R}_i(t)].\end{aligned}\quad (86)$$

A value $M = 200\,000$ was used in Ref. 40 to simulate the desorption of Li and Na atoms excited to the $3s$ and $4s$ states, respectively.

It can be shown that the continuity equation is automatically fulfilled if $\dot{\mathbf{R}}_i(t) = \mathbf{v}[\mathbf{R}_i(t)]$, *i.e.*, if the change in time of the position of the test particle is equal to the velocity field evaluated at the position of that test particle. The equation of motion obeyed by the velocity field –and thus the equation for the trajectories– is obtained by taking the gradient of Eq. (84b). Rewriting it in the Lagrangian reference frame ($d/dt = \partial/\partial t + \mathbf{v} \cdot \nabla_{\mathbf{r}_I}$), one then obtains the “quantum” Newton equation

$$m_I \ddot{\mathbf{R}}_i(t) = - \nabla_{\mathbf{r}_I} [\mathcal{Q}(\mathbf{r}_I, t) + V(\mathbf{r}_I, t)]|_{\mathbf{r}_I=\mathbf{R}_i(t)} . \quad (87)$$

The quantum potential $\mathcal{Q}(\mathbf{r}_I, t)$ is computed using the histogram of test particles as the probability density in the same mesh and using the same n -points formulas for the derivatives as used for the helium distribution.

For illustration purpose, let us consider the 1D, x direction and the evolution of the test particles up to time t . The helium density along the x -axis is represented on a mesh with step size $\Delta = h_x$ from x_{min} (usually negative) to x_{max} . The bin i in which the k test particle with coordinate $x = X_k(t)$ is at time t is determined as

$$i = \text{Integer}\left[\frac{X_k(t) - x_{min}}{h_x}\right] + 1 \quad (88)$$

A unit is added to the i^{th} -bin contents for each test particle which verifies this equation. The same is done in 3D. Dividing by $Mh_xh_yh_z$, one obtains a normalized histogram representing $|\varphi(\mathbf{r}_I, t)|^2$ that is smoothed out as indicated in Eq. (31). Usually, the smoothing is repeated 3 times (notice that it does not alter the normalization) in order to obtain the final probability distribution $|\varphi(\mathbf{r}, t)|^2$.

Both the helium wave function and test particle trajectories aiming at representing the

quantum development of the impurity wave function in Eqs. (43) are consistently computed at each time step. Eq. (43a) and Eq. (87) are solved using the predictor-modified-corrector algorithm previously described.

Expectation values of $\mathbf{r}_I(t)$ and $\mathbf{v}_I(t)$: They are sometimes needed for graphical representations. We have

$$\langle \mathbf{r}_I(t) \rangle = \int d\mathbf{r}_I \mathbf{r}_I \varphi^2(\mathbf{r}_I, t) \quad (89)$$

For $\mathbf{v}_I(t)$ we have

$$\begin{aligned} \langle \mathbf{v}_I(t) \rangle &= \frac{1}{m_I} \int d\mathbf{r}_I \phi^*(\mathbf{r}_I, t) \{-i\hbar \nabla_{\mathbf{r}_I}\} \phi(\mathbf{r}_I, t) \\ &= -i \frac{\hbar}{m_I} \int d\mathbf{r}_I [\varphi(\mathbf{r}_I, t) \nabla_{\mathbf{r}_I} \varphi(\mathbf{r}_I, t) + \varphi^2(\mathbf{r}_I, t) i \nabla_{\mathbf{r}_I} \mathcal{S}(\mathbf{r}_I, t)] \end{aligned} \quad (90)$$

since $\nabla_{\mathbf{r}_I}[\varphi^2(\mathbf{r}_I, t)] = 2\varphi(\mathbf{r}_I, t) \nabla_{\mathbf{r}_I} \varphi(\mathbf{r}_I, t)$,

$$\langle \mathbf{v}_I(t) \rangle = \frac{\hbar}{m_I} \int d\mathbf{r} \varphi^2(\mathbf{r}_I, t) \nabla_{\mathbf{r}_I} \mathcal{S}(\mathbf{r}, t) - i \frac{\hbar}{2m_I} \int d\mathbf{r}_I \nabla_{\mathbf{r}_I} [\varphi^2(\mathbf{r}_I, t)] \quad (91)$$

The second term cancels out since $\varphi(\mathbf{r}_I, t)$ is zero on the surface at infinity and one gets a classical-like expression for $\langle \mathbf{v}_I \rangle$

$$\langle \mathbf{v}_I(t) \rangle = \int d\mathbf{r}_I \mathbf{v}(\mathbf{r}_I, t) \varphi^2(\mathbf{r}_I, t) = \frac{1}{m_I} \int d\mathbf{r}_I \mathbf{j}(\mathbf{r}_I, t) \quad (92)$$

Expressions for other observables can be obtained in a similar way. In particular, the energy of the impurity as a function of time:

$$\begin{aligned} E(t) &= \int d\mathbf{r}_I \Phi^*(\mathbf{r}_I, t) \left[\frac{-\hbar^2}{2m_I} \nabla_{\mathbf{r}_I}^2 + V(\mathbf{r}_I, t) \right] \Phi(\mathbf{r}_I, t) \\ &= \int d\mathbf{r}_I \left[\frac{1}{2} m_I v^2(\mathbf{r}_I, t) + \mathcal{Q}(\mathbf{r}_I, t) + V(\mathbf{r}_I, t) \right] \end{aligned} \quad (93)$$

As an illustrative example, Fig. 10 shows snapshots of the ${}^4\text{He}_{1000}$ density in the (x, z) plane obtained after one He atom (treated as an impurity) located at 20 Å from its center is excited from the $1s$ to the $2s$ state. The evolution of the probability density of the He* atom is also shown (brightest spot).⁵⁸ The number of test particles used for the simulation is $M = 10^6$.

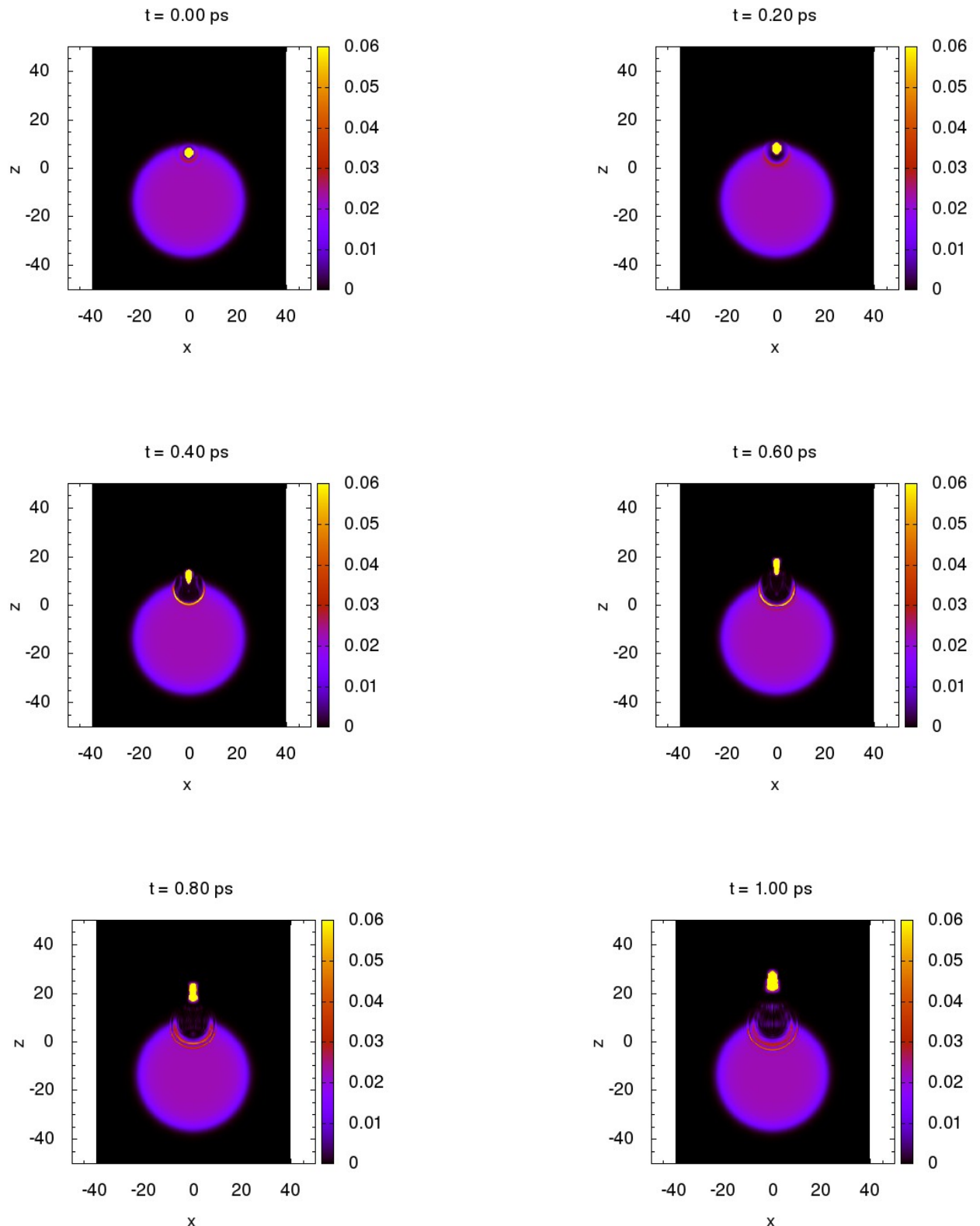


FIG. 10: Snapshots of the He density during the evolution of the $\text{He}^* @ {}^4\text{He}_{1000}$ starting from $\mathbf{r}_X = 20 \text{ \AA}$.

Acknowledgments

This work has been performed under Grants No. FIS2014-52285-C2-1-P from DGI, Spain, and 2014SGR401 from Generalitat de Catalunya. AL has been supported by the ME (Spain) FPI program, Grant No. BES-2012-057439. MB thanks the Université Fédérale Toulouse Midi-Pyrénées for financial support during the completion of this work through the “Chaires d’Attractivité 2014” Programme IMDYNHE.

APPENDIX A: CONVOLUTIONS: EXAMPLE OF THE IMPURITY-HE DROPLET INTERACTION

In this appendix we explain how convolutions are computed in the programs. Convolutions appear in the definition of the density functional [Eq. (8)] and in the impurity-helium potentials for the doped droplet [see Eqs. (18)] when the impurity is treated quantum mechanically. We show here in detail how the convolution to get the potential acting on the quantum impurity in Eq. (18b) is computed, in the case of $L = 0$ angular momentum.

The convolution to calculate this potential is of the form:

$$W(\mathbf{r}_I) = \int d\mathbf{r} V(|\mathbf{r} - \mathbf{r}_I|) \rho(\mathbf{r}) \quad (\text{A1})$$

We use the property of the Fourier transform of a convolution:

$$\text{if } h(\mathbf{r}) = \int d\mathbf{r}' f(\mathbf{r}') g(\mathbf{r} - \mathbf{r}') \quad \text{then} \quad \mathcal{F}[h] = \mathcal{F}[f]\mathcal{F}[g] \quad (\text{A2})$$

where $\mathcal{F}[f]$ is the Fourier transform (FT) of function $f(\mathbf{r})$, defined as:

$$\mathcal{F}[f(\mathbf{r})] = F(\mathbf{q}) = \int d\mathbf{r} e^{i2\pi\mathbf{qr}} f(\mathbf{r}) . \quad (\text{A3})$$

For an $L = 0$ electronic state of the impurity, V is of spherical symmetry, *i.e.* $V(\mathbf{r}) = V(|\mathbf{r}|) = V(r)$. Its FT can then be expressed in spherical coordinates. By choosing the Z axis parallel to \mathbf{q} in order to evaluate it, Eq. (A3) reduces to a single integral by integrating over the angles:

$$\mathcal{F}[V](\mathbf{q}) \rightarrow F(q) = \frac{2}{q} \int_0^\infty r dr V(r) \sin(2\pi qr) , \quad (\text{A4})$$

where $q = |\mathbf{q}|$.

Several steps are taken to make the evaluation of Eq. (A1) as efficient as possible. This is important since its evaluation has to be done at each time step. The first and obvious one is to calculate the FT of the potential (A4) once and for all at the beginning of the propagation.

The other ones make use of known analytical forms for the FT of simple functions. The pair potential $V(r)$ is usually obtained from *ab initio* calculations on a grid of points. It is

then interpolated or fitted to analytical expressions. We use powers of $1/r$ in order to get the correct asymptotic behavior. This requires to screen the potential at short range. This is achieved by making it constant below a given distance r_{cut} , which is chosen such that $V(r_{cut})$ is several 10^3 K. The actual value of the cutoff is rather irrelevant, but it has to be consistently used everywhere once chosen.

In a second step, cubic spline interpolation of the fitted analytical expressions is carried out. This is very useful for two reasons. The FT of the potential is then analytic by pieces, since the integrals (A4) for a cubic polynomial can be deduced from

$$\begin{aligned} \int dx x^n \sin(ax) &= \sum_{k=0}^{2k < n} (-1)^{k+1} \frac{x^{n-2k}}{a^{2k+1}} \frac{n!}{(n-2k)!} \cos(ax) \\ &+ \sum_{k=0}^{2k+1 \leq n} (-1)^k \frac{x^{n-(2k+1)}}{a^{2k+2}} \frac{n!}{(n-2k-1)!} \sin(ax) \end{aligned} \quad (\text{A5})$$

(with $n \leq 3$). The second reason is that we have then a kind of “universal” method, independent of the analytical expression used for the fit, to calculate the FT of the potential. It is then quite straightforward to change potentials, hence test different potentials for the same system, or change system. The (r_{cut}, ∞) region is split in a number of intervals (usually four: the repulsive part from r_{cut} to the point where the potential is zero; the interval from that point to the potential minimum; the interval from the minimum to the inflexion point of the potential; and the interval from the inflexion point to infinite (in practice, 1000 Å)). Within each interval the mentioned cubic spline is carried out. Notice that $F(q = 0)$ is the volume integral of the screened potential and is obtained separately.

APPENDIX B: INTERNAL UNITS OF THE PROGRAMS

In this Appendix we give some details on the units used in the calculations. In the helium functional definition the energy unit is Kelvin and the length unit is Å. In the dynamics the time scale is most often ps, and hence velocities appear in Å/ps, whose equivalence is 100 m/s. Some ingredients such as pair potentials have to be written in these units before being used. The energy scale of the absorption and emission spectra is cm⁻¹.

Let us recall some equivalences and constant values taken from the NIST table of constants (<http://physics.nist.gov/constants>):

- Recall that: 1 Å = 10⁻¹⁰ m; 1 fm = 10⁻¹⁵ m; 1 ps = 10⁻¹² s
- Boltzmann constant: 8.6173303 10⁻⁵ eV/K; this means that 1 eV = 11604.522 K
- 1 cm⁻¹ = 1.43877736 K
- Atomic mass unit: $m_u = 931.4940954 \text{ MeV} = 1.080954 \cdot 10^{13} \text{ K}$
- $\hbar = 6.582119514 \cdot 10^{-16} \text{ eV s} = 7.638235 \text{ K ps}$
- $c = 299792458 \text{ m/s}$
- $\hbar c = 197.3269788 \text{ MeV fm} = 2.289885 \cdot 10^7 \text{ K Å}$
- He mass: $4.002 \times 931.49 = 3727.8 \text{ MeV}$

When solving the effective Schrödinger equation for the superfluid, the \hbar constant has been incorporated into the definition of “time”. This means that we have actually solved the equation

$$i \frac{\partial \Psi}{\partial(t/\hbar)} = \mathcal{H}\Psi$$

For the sake of coherence, this way of handling time has also been adopted for the dynamic evolution of the impurity. As a consequence, what internally is called “velocity” of the impurity (v_{inter}) for instance, instead of being $d\mathbf{r}/dt$ actually is $d\mathbf{r}/d(t/\hbar)$. One may recover the “physical” impurity velocity v_{phys} dividing the internal velocity by \hbar , namely $v_{phys} = v_{inter}/\hbar$. Using $\hbar = 7.638235 \text{ K ps}$, this yields v_{phys} in Å/ps (i.e., in 100 m/s units).

Similarly, in order to obtain the kinetic energy of the impurity I in K, as any other energy printed and/or stored during the dynamics, one has to keep in mind that

$$\frac{1}{2}m_I v_{phys}^2 \rightarrow \frac{1}{2}\frac{m_I}{\hbar^2}v_{inter}^2 \rightarrow \frac{1}{2}\frac{m_I c^2}{(\hbar c)^2}v_{inter}^2$$

Writing the impurity mass in units of m_u , $m_I = M_I m_u$ and taking for M_I the value in atomic mass units as given in the atomic mass list of NIST (which takes into account the natural isotopic composition of the impurity), one obtains the kinetic energy of the impurity in K as

$$E_{kin,I} = \frac{1}{2}M_I \frac{m_u c^2}{(\hbar c)^2}v_{inter}^2 \rightarrow \frac{1}{2}M_I \times 0.02061484 v_{inter}^2 \text{ (K)}$$

since $m_u c^2/(\hbar c)^2 = 0.02061484 \text{ K}^{-1} \text{\AA}^{-2}$. M_I values for the impurities used in some recent applications are *e.g.* $M_{Rb} = 85.4678$; $M_{Cs} = 132.9055$; $M_{Xe} = 131.293$.

Often we evaluate the kinetic energy of the impurity in K from its velocity in hundreds m/s, so better have a simple-to-use expression:

$$E_{kin,I}(\text{K}) = \frac{1}{2}M_I m_u c^2 \left(\frac{v}{c}\right)^2 \rightarrow 0.600 M_I \left(v_{\text{A/ps}}^\circ\right)^2$$

For Cs at 200 m/s, $v^2 = 4$, $M_{Cs} = 132.9055$ and this yields $E_{kin,Cs} \sim 319.3$ K.

APPENDIX C: DETAILS ON VORTEX ARRAY CALCULATIONS

In this Appendix we give some details on the vortex array calculations. A dimensionless angular velocity is defined according to Eq. (2.8) of Brown and Scriven⁵⁹

$$\Omega = \sqrt{\frac{m_{\text{He}} \rho_0 R^3}{8 \gamma}} \omega ,$$

where γ is the surface tension of liquid He, ρ_0 is the atomic saturation density, and R the radius of the droplet of constant density ρ_0 . One may check that Ω is dimensionless. Since $4\pi R^3 \rho_0 / 3 = N$,

$$\Omega = \sqrt{\frac{3 m_{\text{He}} N}{32 \pi \gamma}} \omega = \sqrt{\frac{3}{32 \pi} \frac{m_{\text{He}}}{\hbar^2} \frac{1}{\gamma} N} \hbar \omega$$

Values for ⁴He:

- $\hbar^2/m_{\text{He}} = 12.12 \text{ K \AA}^2$
- $\rho_0 = 0.021836 \text{ \AA}^{-3}$
- $\hbar = 7.638 \times 10^{-12} \text{ K s} = 7.638 \text{ K ps}$
- $\gamma = 0.274 \text{ K \AA}^{-2}$

Substituting values,

$$\Omega = 9.48 \times 10^{-2} \sqrt{N} \frac{\hbar}{\text{K}} \omega \text{ [dimensionless]}$$

This relationship allows one to use a dimensionless frequency Ω to represent the results.¹¹

In particular, if $N = 1000$

$$\Omega = 2.998 \frac{\hbar}{\text{K}} \omega$$

Working in the corotating frame one minimizes $\langle \hat{H} - \omega \hat{L}_z \rangle$ at given ω and N values; to find the most stable configuration one has to compare the value of $\langle \hat{H} - \omega \hat{L}_z \rangle$ for different N_v vortices (there are metastability regions^{10,11}). Since the energy unit is K, the code has to be “fed” with ω values in K/ \hbar units (there is an \hbar hidden in L_z that is not explicit in the code). Using the value of \hbar given above it is easy to transform the angular velocity used in the code into s⁻¹. For instance, the critical frequency for the nucleation of one vortex in the ⁴He₁₀₀₀ droplet given in Eq. (39), $\omega_c = 0.0167 \text{ ps}^{-1}$, should have been introduced into the

code as $0.0167 \times 7.638 = 0.1276$; this makes ωL in K and can thus be added to the energy represented by H . The corresponding Ω_c is 0.382.

APPENDIX D: SPECTROSCOPIC NOTATION FOR $L = 1$ EXCITED ATOMIC STATES IN THE PRESENCE OF A ${}^4\text{He}$ DROPLET

There are different possibilities for fixing the notation of the excited states of the impurity-droplet complex. In this guide we have adhered to what is called the “standard Hund’s case (a) notation” as discussed in *e.g.* Ref. 60. In analogy with diatomic molecules spectroscopy, a local “pseudo-diatomic” frame is defined with its z -axis parallel to the axis from the center of mass of the droplet to the dopant. The electronic states $|L, S, \Lambda, \Sigma\rangle$ are labeled as ${}^{2S+1}\bar{\Lambda}_\Omega$, S being the spin quantum number, Λ , Σ , and $\Omega = \Lambda + \Sigma$ being the projection quantum number of the orbital \mathbf{L} , spin \mathbf{S} and total \mathbf{J} [Eq. (55)] electronic angular momentum, respectively, onto the local z axis. The diatomic notation $\bar{\Lambda} \equiv \Sigma, \Pi, \Delta\dots$ is used for $\Lambda = 0, \pm 1, \pm 2\dots$ Diagonalization of $H^{\text{He}-I}$ [Eq. (58)] yields six eigenstates that are two-fold degenerate due to Kramer’s theorem.^{43,61} Note that within cylindrical symmetry, Ω is a “good” quantum number. Hence (in the limit where other n states of the atom can be neglected) the $|J = 3/2, \Omega = \pm 3/2\rangle$ atomic states do not mix with the others and correlate with the ${}^2\Pi_{3/2}$ atomic states at long distance. Only the ${}^2\Pi_{1/2}$ and ${}^2\Sigma_{1/2}$ states can be mixed by spin-orbit coupling. Since Σ interaction is more repulsive than Π interaction, the ${}^2\Sigma_{1/2}$ is the highest one in energy and correlates asymptotically to the $|J = 3/2, \Omega = \pm 1/2\rangle$ upper atomic states, while the ${}^2\Pi_{1/2}$ states correlate with the lower $|J = 1/2, \Omega = \pm 1/2\rangle$ atomic states.

* Electronic address: mbg@fqa.ub.edu

† Electronic address: Nadine.Halberstadt@irsamc.ups-tlse.fr

‡ Electronic address: marti@fqa.ub.edu

- ¹ M. PI, F. ANCILOTTO, F. COPPENS, N. HALBERSTADT, A. HERNANDO, A. LEAL, D. MATEO, R. MAYOL, and M. BARRANCO, 4He-DFT BCN-TLS: A Computer Package for Simulating Structural Properties and Dynamics of Doped Liquid Helium-4 Systems, Available: <https://github.com/bcntls2016/>, 2016.
- ² M. WEISSBLUTH, *Atoms and molecules*, Academic Press, New York, 1980.
- ³ B. H. BRANSDEN and C. J. JOACHAIN, *Physics of atoms and molecules*, Longman Scientific & Technical, Longman House, Burnt Mill, Harlow, Essex CM20 2JE, England, 1990.
- ⁴ D. TANNOR, *Introduction to Quantum mechanics: A Time-Dependent Perspective*, University Science Books, Sausalito, California, 2007.
- ⁵ F. O. ELLISON, *J. Am. Chem. Soc.* **85**, 3540 (1963).
- ⁶ F. ANCILOTTO, M. BARRANCO, F. COPPENS, J. ELORANTA, N. HALBERSTADT, A. HERNANDO, D. MATEO, and M. PI, *Int. Review in Phys. Chem.* , to be published (2017).
- ⁷ R. J. DONNELLY, in *Quantized vortices in helium II*, volume 3, Cambridge Studies in Low Temperature Physics (Cambridge University Press), Cambridge, U.K, 1991.
- ⁸ L. PITAEVSKII and S. STRINGARI, in *Bose-Einstein Condensation*, volume 116, Clarendon, International Series of Monographs on Physics, Oxford, U.K, 2003.
- ⁹ M. PI, R. MAYOL, A. HERNANDO, M. BARRANCO, and F. ANCILOTTO, *J. Chem. Phys.* **126**, 244502 (2007).
- ¹⁰ F. ANCILOTTO, M. PI, and M. BARRANCO, *Phys. Rev. B* **90**, 174512 (2014).
- ¹¹ F. ANCILOTTO, M. PI, and M. BARRANCO, *Phys. Rev. B* **91**, 100503(R) (2015).
- ¹² F. DALFOVO, R. MAYOL, M. PI, and M. BARRANCO, *Phys. Rev. Lett* **85**, 1028 (2000).
- ¹³ F. DALFOVO, A. LASTRI, L. PRICAUPENKO, S. STRINGARI, and J. TREINER, *Phys. Rev. B* **52**, 1193 (1995).
- ¹⁴ R. J. DONNELLY, J. A. DONNELLY, and R. N. HILLS, *J. Low Temp. Phys.* **44**, 471 (1981).
- ¹⁵ F. ANCILOTTO, M. BARRANCO, and M. PI, *Phys. Rev. B* **82**, 014517 (2010).
- ¹⁶ E. POPOV and J. ELORANTA, *J. Chem. Phys.* **142**, 204704 (2015).

- ¹⁷ F. ANCILOTTO, M. BARRANCO, F. CAUPIN, R. MAYOL, and M. PI, *Phys. Rev. B* **72**, 214522 (2005).
- ¹⁸ S. STRINGARI and J. TREINER, *J. Chem. Phys.* **87**, 5021 (1987).
- ¹⁹ S. STRINGARI and J. TREINER, *Phys. Rev. B* **36**, 16 (1987).
- ²⁰ D. MATEO, D. JIN, M. BARRANCO, and M. PI, *J. Chem. Phys.* **134**, 044507 (2011).
- ²¹ F. ANCILOTTO, F. FACCIN, and F. TOIGO, *Phys. Rev. B* **62**, 17035 (2000).
- ²² M. BARRANCO, M. PI, S. M. GATICA, E. S. HERNÁNDEZ, and J. NAVARRO, *Phys. Rev. B* **56**, 8997 (1997).
- ²³ A. LEAL, D. MATEO, M. PI, M. BARRANCO, and J. NAVARRO, *J. Chem. Phys.* **139**, 174308 (2013).
- ²⁴ A. HERNANDO, R. MAYOL, M. PI, M. BARRANCO, F. ANCILOTTO, O. BÜNERMANN, and F. STIENKEMEIER, *J. Phys. Chem. A* **111**, 7303 (2007).
- ²⁵ E. S. HERNÁNDEZ and J. NAVARRO, in *Microscopic approaches to quantum liquids in confined geometries*, edited by E. KROTSCHEK and J. NAVARRO, p. 261, World Sci., Singapore, 2002.
- ²⁶ M. ABAD, M. GUILLEUMAS, R. MAYOL, M. PI, and D. M. JEZEK, *Phys. Rev. A* **81**, 043619 (2010).
- ²⁷ F. ANCILOTTO, M. BARRANCO, J. NAVARRO, and M. PI, *J. Low Temp. Phys.* (2016).
- ²⁸ M. FRIGO and S. G. JOHNSON, *Proc. IEEE* **93**, 216 (2005).
- ²⁹ A. GOLDBERG and J. L. SCHWARTZ, *J. Comp. Phys.* **1**, 433 (1967).
- ³⁰ A. GOLDBERG and J. L. SCHWARTZ, *J. Comp. Phys.* **1**, 448 (1967).
- ³¹ F. ANCILOTTO, P. B. LERNER, and M. W. COLE, *J. Low Temp. Phys.* **101**, 1123 (1995).
- ³² W. H. PRESS, S. A. TEUKOLSKY, W. T. VETTERLING, and B. P. FLANNERY, *Numerical Recipes*, Cambridge University Press, Cambridge, 1992.
- ³³ T. HOSHI, M. ARAI, and T. FUJIWARA, *Phys. Rev. B* **52**, R5459 (1995).
- ³⁴ F. DALFOVO and S. STRINGARI, *Phys. Rev. A* **53**, 2477 (1996).
- ³⁵ J. VON VANGEROW, A. STIEG, F. STIENKEMEIER, M. MUDRICH, A. LEAL, D. MATEO, A. HERNANDO, M. BARRANCO, and M. PI, *J. Phys. Chem. A* **118**, 6604 (2014).
- ³⁶ D. MATEO, A. LEAL, A. HERNANDO, M. BARRANCO, M. PI, F. CARGNONI, M. MELLA, X. ZHANG, and M. DRABBELS, *J. Chem. Phys.* **140**, 131101 (2014).
- ³⁷ A. LEAL, D. MATEO, A. HERNANDO, M. PI, M. BARRANCO, A. PONTI, F. CARGNONI, and M. DRABBELS, *Phys. Rev. B* **90**, 224518 (2014).

- ³⁸ F. COPPENS, A. LEAL, M. BARRANCO, N. HALBERSTADT, and M. PI, *J. Low Temp. Phys.*, , (accepted.) (2016).
- ³⁹ R. E. WYATT, *Quantum Dynamics with Trajectories*, Springer, New York, 2005.
- ⁴⁰ A. HERNANDO, M. BARRANCO, M. PI, E. LOGINOV, M. LANGLET, and M. DRABBELS, *Phys. Chem. Chem. Phys.* **14**, 3996 (2012).
- ⁴¹ D. MATEO, A. HERNANDO, M. BARRANCO, E. LOGINOV, M. DRABBELS, and M. PI, *Phys. Chem. Chem. Phys.* **15**, 18388 (2013).
- ⁴² A. HERNANDO, M. BARRANCO, R. MAYOL, M. PI, and M. KROŚNICKI, *Phys. Rev. B* **77**, 024513 (2008).
- ⁴³ P. H. E. MEIER and E. BAUER, *Group Theory*, North-Holland, Amsterdam, 1962.
- ⁴⁴ A. LEAL and ET AL, to be published, 2016.
- ⁴⁵ A. RALSTON and H. S. WILF, *Mathematical methods for digital computers*, John Wiley and Sons, New York, 1960.
- ⁴⁶ C. LEFORESTIER and R. E. WYATT, *J. Chem. Phys.* , 2334 (1983).
- ⁴⁷ A. VIBÓK and G. G. BALINT-KURTI, *J. Phys. Chem.* **96**, 8712 (1992).
- ⁴⁸ S. H. PATIL, *J. Chem. Phys.* **94**, 8089 (1991).
- ⁴⁹ J. PASCALE, *Phys. Rev. A* **28**, 632 (1983).
- ⁵⁰ S. STIENKEMEIER, F. MEIER, and H. O. LUTZ, *Eur. Phys. J. D* **9**, 313 (1999).
- ⁵¹ D. MATEO, A. HERNANDO, M. BARRANCO, R. MAYOL, and M. PI, *Phys. Rev. B* **83**, 174505 (2011).
- ⁵² A. HERNANDO, M. BARRANCO, R. MAYOL, M. PI, F. ANCILOTTO, O. BÜNERMANN, and F. STIENKEMEIER, *J. Low Temp. Phys.* **158**, 105 (2010).
- ⁵³ R. SCHINKE, *Photodissociation dynamics*, Cambridge University Press, Cambridge, UK, 1995.
- ⁵⁴ A. KRAMIDA, YU. RALCHENKO, J. READER, and AND NIST ASD TEAM, NIST Atomic Spectra Database (ver. 5.3), [Online]. Available: <http://physics.nist.gov/asd> [2017, January 14]. National Institute of Standards and Technology, Gaithersburg, MD., 2015.
- ⁵⁵ M. MELLA and F. CARGNONI, *J. Phys. Chem. A* **118**, 6473 (2014).
- ⁵⁶ D. NETTELS, A. HOFER, P. MOROSHKIN, R. MÜLLER-SIEBERT, S. ULZEGA, and A. WEIS, *Phys. Rev. Lett.* **94**, 063001 (2005).
- ⁵⁷ R. A. AZIZ and A. R. JANZEN, *Phys. Rev. Lett.* **74**, 1586 (1995).
- ⁵⁸ M. BARRANCO, J. ELORANTA, A. HERNANDO, and M. PI, unpublished, 2016.

- ⁵⁹ R. A. BROWN and L. E. SCRIVEN, *Proc. R. Soc. London, Ser. A* **371**, 331 (1980).
- ⁶⁰ A. PIFRADER, O. ALLARD, G. AUBÖCK, C. CALLEGARI, W. E. ERNST, R. HUBERT, and F. ANCILOTTO, *J. Chem. Phys.* **133**, 164502 (2010).
- ⁶¹ A. NAKAYAMA and K. YAMASHITA, *J. Chem. Phys.* **114**, 780 (2001).
- ⁶² As specified at the beginning of the introduction, the photoexciting or photoionizing laser pulse is assumed to be short enough that the atomic nuclei do not move significantly, but long enough that its width in energy only covers the desired electronic state.